Study of the Deep Chlorophyll Maximum in the Black Sea as seen from Biogeochemical-Argo floats

Auteur : Ricour, Florian
Promoteur(s) : Gregoire, Marilaure; 3818
Faculté : Faculté des Sciences
Diplôme : Master en océanographie, à finalité approfondie
Année académique : 2017-2018
URI/URL : http://hdl.handle.net/2268.2/4931

Study of the Deep Chlorophyll Maximum in the Black Sea as seen from Biogeochemical-Argo floats

A Thesis Submitted in Partial Fulfillment of the Requirements for the Master's Degree in Oceanography

Author
FLORIAN RICOUR

Supervisors
MARILAURE GRÉGOIRE
FABRIZIO D'ORTENZIO

ACADEMIC YEAR 2017-2018

UNIVERSITY OF LIÈGE
FACULTY OF SCIENCES

Conformément aux règles imposées à la rédaction, ce mémoire ne doit pas dépasser 50 pages, rédigées en Times 12 ou équivalent.

ACKNOWLEDGMENTS

I would like to thank my supervisor, Marilaure Grégoire, for guiding me throughout the year on this project, for giving me the opportunity to work in stimulating environments as well as with excellent researchers and for helping me during the redaction, improving without a doubt the quality of this document.

I would like to thank my supervisor at the LOV, Fabrizio D'Ortenzio, for his help, support and availability, even on the Téthys II.

I would also like to thank Arthur Capet for his help with *R* and for our numerous discussions, inside or outside meetings, always in a great atmosphere.

I would especially like to thank Charles Troupin for his help with *DIVAnd* and for reading my manuscript, greatly improving its content.

I would like to thank Bruno Delille for his help before and after the cruise and especially for his availability.

I would also like to thank the R/V Akademik crew and especially Nataliya Slabakova, Violeta Slabakova and Kremena Stefanova.

I would like to thank Antoine Poteau for his help with the BGC-Argo float.

I would especially like to thank Marin for our discussions on the DCM and for his pieces of advice as well as Marine and Jenna for reading this document.

I would also like to thank Louis, Romain, Benjamin and Loïc for making me feel at home.

Finally, I would like to thank my family for allowing me to pursue my objectives, my brother for reading this document and my friends for their support.

Contents

1 Summary

La Mer Noire est une zone océanique tout à fait particulière, représentant le plus grand bassin anoxique de la planète. Le déploiement de flotteurs biogéochimiques dans le cadre du projet Argo a permis d'augmenter considérablement la quantité de données disponibles et plus particulièrement le nombre de profils de chlorophylle a. Ces derniers ont subi différents contrôles de qualité ainsi qu'une correction en profondeur, là où la matière organique dissoute colorée semble pertuber au plus le fluorimètre mesurant la fluorescence de la chlorophylle a. Une nouvelle méthode de correction de l'augmentation du signal de chlorophylle a en profondeur, se basant sur un profil virtuel de matière organique dissoute colorée, a également été exposée.

D'autre part, l'étude du maximum de chlorophylle a observé en subsurface a montré que ce dernier se forme après l'efflorescence algale se produisant généralement à la fin de l'hiver ou au début du printemps. Ensuite, il se maintient jusqu'à la fin de l'été pour être progressivement érodé avant de disparaitre avant le début de l'hiver, quand la profondeur de la couche de mélange augmente à nouveau. Enfin, il semble que ce maximum soit lié à l'anomalie de densité potentielle de la couche de mélange de l'hiver précédent, où une efflorescence algale s'est produite. Contrairement à d'autres hypothèses de formation de ce pic en subsurface, aucun lien clair n'a été fait avec la lumière comme élément moteur de ses variations verticales dans la colonne d'eau.

*

The Black Sea is a peculiar oceanic environment, representing the largest anoxic basin on the planet. The deployment of biogeochemical floats in the frame of the Argo project has allowed to considerably increase the quantity of available data and especially the number of chlorophyll a profiles. The latter were quality controlled using specific procedures and were corrected at depth, where the colored dissolved organic matter seems to perturb at most the fluorometer measuring chlorophyll a fluorescence. A new correction method addressing the increase of the chlorophyll a signal at depth, based on a virtual profile of colored dissolved organic matter, has also been introduced.

On the other hand, the study of the chlorophyll maximum observed in subsurface has shown that the latter forms after the late winter/early spring bloom. Then, this maximum is well established until the end of summer where it is progressively eroded before disappearing in late autumn, when the depth of the mixed layer increases again. Finally, it seems that this maximum is governed by the potential density anomaly of the previous winter mixed layer, where a bloom occurred. Contrarily to other studies on the formation of this subsurface peak, no clear link has been made with light as driving process for its vertical variations in the water column.

2 Introduction

2.1 The Black Sea

The Black Sea is a marginal sea located in the southeastern part of Europe (between 40°55' - 46°32'N and 27°27' - 41°32'E). It is connected to the Mediterranean Sea through the Bosphorus Strait and to the Azov Sea in the north through the Kertch Strait. The Black Sea has a surface area of 4.2 10^5 km^2 and an average depth of 1240 m (max. 2300 m) (Özsoy and Ünlüata, 1997). The circulation consists of three major currents (Bakan and Byükgüngör, 2000; Kubryakov et al., 2016): the Rim Current (cyclonic current) which flows along the basin's periphery (continental slope), the Western cyclonic gyre and the Eastern cyclonic gyre (Figure 1). By 2000, 90% of its water mass was anoxic (Bakan and Byükgüngör, 2000). The permanent and strong stratification, due to a steep halocline induced by fresh surface waters ($\approx$ 18 PSU) from river inputs versus more saline waters ($\approx$ 23 PSU) of Mediterranean influence below (Özsoy and Ünlüata, 1997; Stanev, 1990), splits the water column into a well oxygenated surface layer from 0 to 50-200 m and a deeper stagnant anoxic layer from 50-200 m down to the bottom. The thickness of the oxic layer differs from the central basin (70-100 m) to the peripheral areas (120-200 m) (Yakushev et al., 2008). However, He et al. (2012) pointed out the fact that the oxic layer rarely goes beyond 100 m but instead is closer to 50-60 meters deep. As the oxygen concentration in the upper layer of the Black Sea depends mostly on physical parameters (oxygen solubility, gas exchange, etc.) and on primary production, it will thus show both temporal (seasonal and interannual) and spatial variations explaining the broad range of depths observed (Konovalov and Murray, 2001).

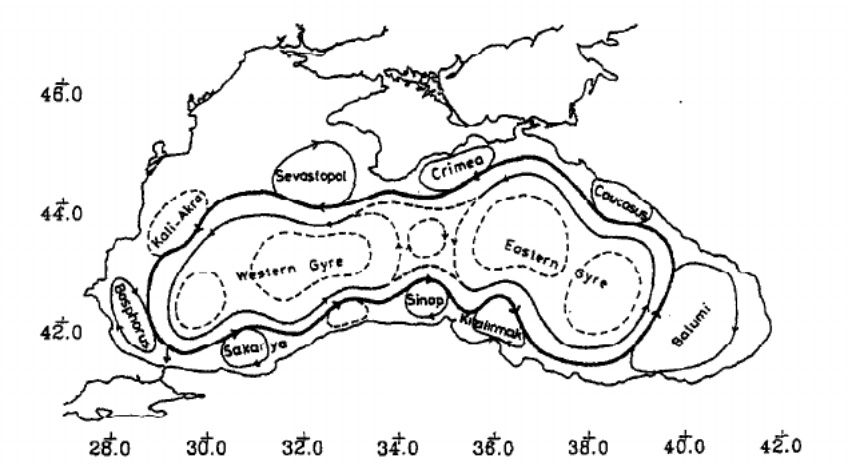

Figure 1: Main circulation patterns. After Özsoy and Ünlüata (1997).

In situ observations of the Black Sea from cruises are mostly near-shore and temporally irregular (Palazov et al., 2014) showing the importance of the Argo Program to the study of the Black Sea biogeochemical and physical characteristics, especially in the context of global warming. The latter could enhance the vertical stratification, decreasing again the ventilation in the deeper layer hence impacting the oxygen content (He et al., 2012; Capet et al., 2016).

2.2 The Argo program

Due to undersampling (both spatial and temporal) from research vessels and because satellite data are typically limited at best (cloud-free periods) to the upper one-fifth of the euphotic zone (Claustre et al., 2009; Johnson et al., 2009; Böhm et al., 2016) which itself fluctuates, there is a lack of *in situ* data in the world's ocean, especially for biology and biochemistry. In order to cope with this issue, autonomous platforms have been deployed to study the ocean biogeochemistry (vertical distribution) at a higher spatial and temporal frequency thus covering the wide spatio-temporal range of oceanic processes for approximately 300 cycles (IOCCG, 2011), *i.e.* typically 5 years up to 8 years. For instance, it will help to extend satellite data into the ocean interior and to highlight trends relevant to climate change (IOCCG, 2011). The Argo program consists of an array of autonomous profiling floats (Fig. 2) enabling continuous, real-time subsurface observations (Roemmich et al., 2009) up to 2000 m. 3000 floats were deployed by the end of 2007.

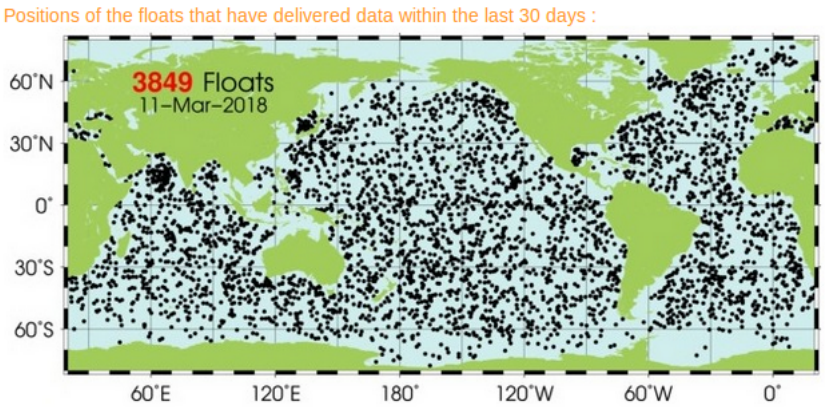

Figure 2: Argo floats cover (11-03-2018). Source: http://www.argo.ucsd.edu/

The concept of an Argo float simply relies on Archimedes's principle. In order to ascend (or descend), a float changes its buoyancy by pumping oil into an external bladder (or by deflating the bladder). This procedure allows the float to increase (or decrease) its volume at a constant mass (Johnson et al., 2009). Their lateral movement, called drift, at a parking depth (typically 1000 m for 5 to 10 days) is governed by currents (see for instance Figure 4). Once a float gets to the surface, it transmits its data and its position to satellites, preferably through Iridium communication (instead of Argos) which is faster and bidirectional hence decreasing the time spent at the surface. This is mostly important for floats equipped with optical sensors in order to avoid sensor drift. The aforementioned effect results from a time-dependent relationship of the measured value, commonly a linear increase or decrease with time, an offset or both (Wong et al., 2018). Biogeochemical-Argo floats (hereafter referred to as BGC-Argo) are now equipped, in addition to the classical CTD, with biogeochemical sensors (*e.g.* oxygen, nitrate, chlorophyll a (Chla), suspended particles and downwelling irradiance sensors (Biogeochemical-Argo Planning Group, 2016)).

2.3 Deep Chlorophyll Maximum

The Deep Chlorophyll Maximum (DCM), also known as the Subsurface Chlorophyll Maximum (Cullen, 2015) is a common feature in the world's ocean (Anderson, 1969; Cullen, 1982; Furuya, 1990; Parslow et al., 2001; Huisman et al., 2006; Ardyna et al., 2013). It is characterized by a subsurface layer of high Chla concentration (*e.g.* Fig. 3). It has been studied for more than 60 years and its processes of formation

and maintenance are still not clearly explained yet (Cullen, 2015). Indeed, it has been shown that Deep Chlorophyll Maxima (DCM) formation can be due to several processes (see for example the comprehensive review of Cullen (2015)). In addition to its origin, the nature itself of the DCM is variable (Cullen, 1982). Multiple hypotheses have been suggested to explain this phenomenon. For instance, it has been hypothesized that the depth of the DCM is related to a thin layer where the growth of phytoplankton (*i.e.* phytoplankton biomass) is maximum (Varela et al., 1992; Estrada et al., 1993; Beckmann and Hense, 2007; Mignot et al., 2014). However, DCM could also form as a result of a shift in the Chla to phytoplankton carbon content (Chla:C_p), meaning that the Chla content of a cell is changing regarding the physiological status of the organism or its physical environment, especially light exposition conditions. This physiological adaptation known as photoacclimatation explains why a DCM is not necessarily a biomass peak (Fennel and Boss, 2003) and can either be an enhancing mechanism for species adapted to low light intensities (Fennel and Boss, 2003; Dubinsky and Stambler, 2009) or a protective mechanism at high irradiance intensities near the water surface (Marra, 1997; Xing et al., 2012a). Other formation hypotheses stated that a DCM can occur due to a decrease in the sinking rate of phytoplankton which could be related either to an aggregation of motile phytoplankton (Cullen, 1985) or to an aggregation of nonmotile phytoplankton at a particular density, *i.e.* whose cells are regulated by buoyancy (Richardson and Cullen, 1995). Differential grazing (Macedo et al., 2000) and other theories have also been proposed Cullen (2015). Thus, it can be easily understood that a DCM results from strong interactions between both biological and physico-chemical variables. These attempts to explain the formation and the maintenance of the DCM illustrate the importance (*e.g.* for the primary production hence for trophic ecosystems (Ardyna et al., 2013)) of such a feature in the global ocean (Navarro and Ruiz, 2013) which accounts up to 80-90% of the total Chla in the water column (Vedernikov and Demidov, 1997).

On the other hand, Yilmaz et al. (1994) showed that the depth of the DCM and its intensity are highly variable and dynamic. They observed in the Mediterranean Sea that the DCM stayed peculiarly within a narrow range of isopycnal surfaces. This particularity was also observed by Ediger and Yilmaz (1996). Moreover, Macedo et al. (2000) emphasized the fact that the characteristics of a DCM are related to both its history and actual environment (biological and physico-chemical conditions). These observations seem to have led to a new hypothesis suggested by Navarro and Ruiz (2013) which takes into account an hysteresis effect. In their paper, they explain that the strong coupling observed between isopycnal surfaces and DCM, in temperate regions, can be explained by taking into account the seasonal history of the water column. Indeed, they found that spring and summer DCM were located at a density relatively close to the one of the previous winter mixed layer. In fact, they showed that DCM were constrained around a potential density anomaly value (σ_θ) which itself depended on the history of the water column (*i.e.* σ_θ of the previous winter mixed layer). Eventually, they describe this hypothesis as the fact that "rather than passively reacting to instant external forcing, DCM modify the physical and chemical environment in such a way that they become self-preserving biological structures". In other words, once a DCM occurs at a specific potential density anomaly, it is constrained at that σ_θ in spite of the depth variability because the DCM itself controls the light-nutrient distribution for phytoplankton. Their research gathered temperate regions (Atlantic/Pacific Oceans and Mediterranean Sea) but no data from the Black Sea were included. The recent deployment of BGC-Argo floats in the Black Sea has allowed to investigate the dynamics of biogeochemical parameters (Stanev et al., 2013, 2014, 2018). In this manuscript, we will use data from BGC-Argo floats collected

since 2014 in order to study the dynamics of the DCM in the Black Sea. We will firstly analyze Chla profiles to identify general characteristics in their vertical structure. Then, we will determine the duration of the DCM and its spatio-temporal variability with depth and density. In the Black Sea, it is well known that biogeochemical properties (*e.g.* nutrients, oxygen, sulfide) show rather constant characteristics through time and space when plotted against density (Konovalov and Murray, 2001; Stanev et al., 2013, 2018). We will show if this statement also applies to the DCM. With that aim, the horizontal distribution of DCM with depth and density will be studied using the *DIVAnd* software tool (n-dimensional Data Interpolating Variational Analysis). Based on these analyses, we will conclude on the hypothesis that best explains the formation of the DCM in the Black Sea.

2.4 Chla profiles correction in the Black Sea

When a photon is absorbed by a Chla molecule, another one (less energetic) is almost immediately re-emitted allowing the molecule to return to its ground state. This process is called fluorescence (Lorenzen, 1966) and it has been used for the measurement of in vivo chlorophyll concentration for a long time (IOCCG, 2011; Schmechtig et al., 2016). Chla is known to be a proxy for phytoplankton biomass (*e.g.* Cullen, 1982) and is now widely measured with fluorometers mounted on autonomous platforms (Johnson et al., 2009). Nevertheless, the conversion from fluorescence to Chla is not always precise due to, for instance, variable pigment/carbon ratio, fluorescence/chlorophyll ratio caused by non-photochemical quenching (NPQ) - a photoprotective mechanism resulting in a decrease in the fluorescence signal at the surface due to light exposition in order to avoid cell damage (Xing et al., 2012a) -, species composition and physiology, temperature, etc. (Claustre et al., 2009; Xing et al., 2011, 2012a) but also from the sensor itself due to the contribution to fluorescence of other particles and/or substances (*e.g.* phaeopigments) (Proctor and Roesler, 2010). What is more, Chla concentration can be highly variable, from 0 to $\sim$ 50 mg m^{-3} (Schmechtig et al., 2014) thus the sensor has to cover this range with a high sensitivity (IOCCG, 2011). Bio-optical sensors are also known to be sensitive to bio-accumulation (acting as quenchers) and bio-fouling, both affecting the fluorescence signal. Consequently, the relationship between fluorescence and chlorophyll is not straightforward.

Moreover, non-zero values are commonly observed at depth where chlorophyll concentrations should be null, typically in the case of non-mixed waters (Schmechtig et al., 2014). Generally, it is assumed that this offset is due to the sensor and a constant value is removed from the profile. However, while this assumption is ordinarily correct, it appears that it is not always true, especially in anoxic environments (Claustre et al., 2008; Schmechtig et al., 2014; Stanev et al., 2017). As such, an increase of the Chla concentration in the deeper part of the water column has been observed in some parts of the world and especially in the Black Sea (*e.g.* Xing et al., 2017) where the Chla concentration should be equal to zero (Fig. 3). Cullen (1982) already stipulated that degradation products of Chla could affect the fluorescence signal while Claustre et al. (2008) mentioned that oxygen-limited conditions might alter the degradation of particulate matter which could lead to such an increase.

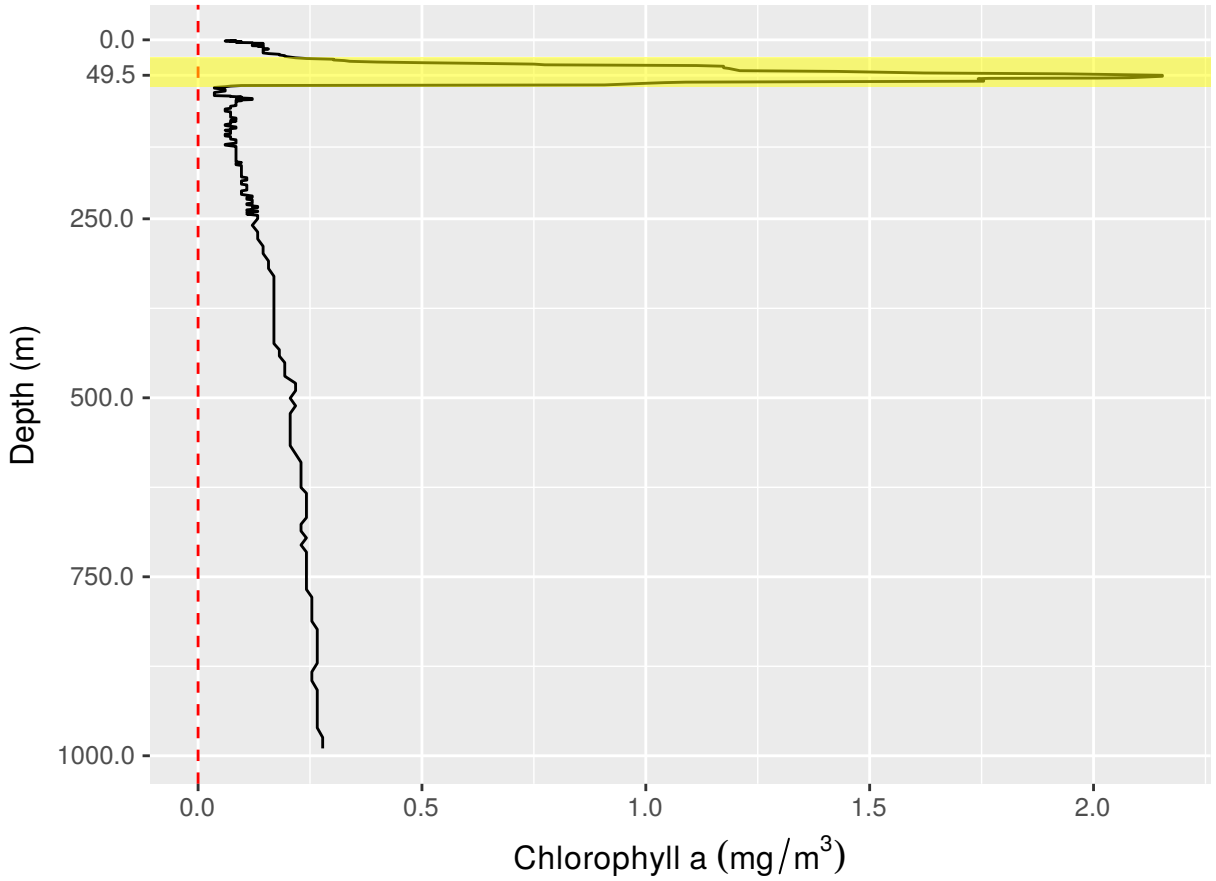

Figure 3: Chla profile measured by the World Meteorological Organization (WMO) float identifier 7900591 on the 21-04-2014. A monotonous increase of Chla occurs at depth while the DCM is located in the yellow area with a peak at 49.5 m.

In fact, this increase would more likely be related to what has been called: "deep sea red fluorescence" (*e.g.* Röttgers and Koch, 2012). The latter feature would be due to fluorescence contamination from fluorescent dissolved organic matter also referred as colored or chromographic dissolved organic matter (CDOM) (Proctor and Roesler, 2010; Xing et al., 2017) and also known as yellow substance (Xing et al., 2012b), humic substance or gelbstoff (Coble et al., 1998). However, one has to keep in mind that fluorescent non-algal particles (particulate detrital material) can also contribute to the fluorescence signal but splitting the contribution of those two sources is not obvious (Röttgers and Koch, 2012; Xing et al., 2017). Deep CDOM concentrations could result from several processes including: *in situ* biological production, release of fluorescent compounds resulting from solubilization under anoxic conditions, diffusion of fluorescent components through the sediments, weak degradation of fluorescent material in absence of oxygen or high fluorescent compounds production from organisms in anoxic conditions (Coble et al., 1991; Para et al., 2010). CDOM can also be brought by riverine runoffs (allochtonous influx) or by phytoplankton degradation, phytoplankton growth, bacterial release/excretion or zooplankton grazing (Coble et al., 1998; Steinberg et al., 2004; Zhang et al., 2009).

On the 29th of March 2018, a BGC-Argo float equipped with biogeochemical sensors (especially Chla and CDOM fluorometers) was deployed in the western Black Sea. Water samples were taken conjointly to the float deployment and were analyzed with High Performance Liquid Chromatography (HPLC) in order to

validate the FDOM-based method (fluorescent dissolved organic matter) implemented by Xing et al. (2017) to correct Chla profiles impacted by red fluorescence. This method relies on the fact that the contribution of CDOM to Chla fluorescence varies (and increases) with depth and should be better than the usual deep-offset correction applied in such cases. The validation of this method with *in situ* data will assess the quality of this correction and will be used to correct profiles prior to DCM analysis. It could also help to define a regional test in the future (Schmechtig et al., 2014). Eventually, a new method based on existing CDOM profiles at the basin scale will be implemented by creating a virtual CDOM profile, representative of CDOM concentrations in the Black Sea, for floats which do not possess a CDOM flurometer. We will show that this new method is rather robust and could potentially be adapted to other regions, increasing the number of exploitable Chla profiles.

3 Material and method

3.1 Study area

The area of study of BGC floats is composed of the western and eastern deep sections of the Black Sea (Fig. 4). Shallower sections and the northwestern continental shelf are thus not taken into account.

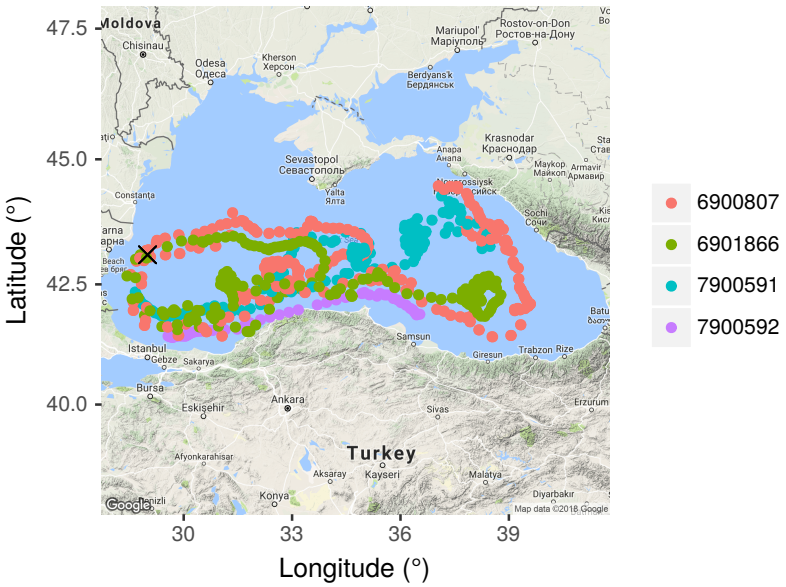

Figure 4: Floats trajectories during the 2014-2017 period. The black cross represents the location of the deployment of the new float (WMO 6903240).

3.2 Data for DCM analyses

Data from 4 BGC-Argo floats (WMO 6900807, 6901866, 7900591 and 7900592) were downloaded from ftp://ftp.ifremer.fr/ifremer/argo/dac/coriolis/ (in NetCDF format) for a period spanning from the 1st January 2014 to the 31th December 2017. During this 4-year period, the 4 floats recorded 847 profiles distributed as shown in Fig. 4.

3.2.1 Data quality

First of all, Chla profiles, or equivalently fluorescence profiles, were quality controlled by removing depths associated to bad data (Quality Control (QC) = 4 (Argo Data Management Team, 2017; Schmechtig et al., 2014)) and were smoothed with a 5-point moving median filter to remove positive spikes suspected to be irrelevant from a biological point of view. Data associated to QC = 3 (probably bad data or bad data that are potentially correctable) were retained. Indeed, due to the increase of Chla at depth in the Black Sea, data are automatically flagged as probably bad data because the new estimation of the Chla dark signal (Chla value measured by the fluorometer in the absence of Chla) is found to have greatly changed compared to its factory calibration (Schmechtig et al., 2014). Also, it has been chosen to remove descent profiles (213 profiles removed) due to two reasons: on the one hand, the time interval between ascent and descent profiles, respectively, was too brief to bring real additional information. On the other hand, the starting depth of such profiles was considerably below the surface, inducing issues with mixed layer depth (MLD) computation which plays a key role in the correction of the NPQ effect. In that perspective, ascending profiles with a starting depth deeper than 5 m were also removed (6 profiles removed). In fact, this criterion removed 5 'stuck' profiles where all values were at the same depth (see also QC on pressure, *i.e.* pressure increasing test). Conjointly, temperature and salinity profiles were also quality controlled (Wong et al., 2018) before computing density profiles. This quality check resulted in the loss of 6 more profiles. Density profiles were computed by using the potential density anomaly referenced at the sea surface and defined by the Thermodynamic Equation Of Seawater (TEOS) of 2010 (IOC, SCOR and IAPSO, 2010). One has to pay attention that this equation uses absolute salinity (g kg^{-1}) and conservative temperature to compute the potential density anomaly.

All four floats are equipped with fluorometers (*WET Labs ECO*) for Chla fluorescence measurements but only two of them also possess a CDOM fluorometer (WMO 6900807 and 6901866). Consequently, two methods for Chla profiles correction will be used: the FDOM-based method (Fig. 5) for floats having a CDOM sensor and the minimum-offset method for the others. Both methods are described in details in Xing et al. (2017). The first one is briefly introduced in Equation 1:

$$FChla_{cor} = FChla_{meas} - FChla_{dark} - Slope_{FDOM} * (FDOM_{meas} - FDOM_{dark}) \quad (1)$$

where $FChla_{cor}$ is the corrected Chla, $FChla_{meas}$ the Chla measured by the *in situ* fluorometer, $FChla_{dark}$ the Chla dark signal, $FDOM_{meas}$ the CDOM measured by the *in situ* fluorometer and $FDOM_{dark}$ the CDOM dark signal (CDOM fluorescence measured in the absence of CDOM). All values are provided after conversion from fluorescence values (in voltage or digital counts) with parameters provided by the manufacturer of each sensor, in mg m^{-3} for Chla and in ppb for CDOM. $Slope_{FDOM}$ represents the intensity of the CDOM fluorescence contamination signal measured by the Chla fluorometer and its units are given in mg m^{-3} ppb^{-1}. Thus, a first hypothesis is being made, stating that the perturbation signal from CDOM is constant with depth. The second method used in this study, the minimum-offset method, has been preferred to the deep-offset method (Schmechtig et al., 2014) due to the significant increase of Chla with depth in the Black Sea. Indeed, the deep-offset method only removes a constant value (*i.e.* the value of the Chla minimum) from the Chla profile at each depth while the minimum-offset method removes this constant above the Chla minimum and sets the profile to zero below. Consequently, this choice will have strictly no

impact on the position of the DCM. That being said, for FDOM-based corrected profiles, the equation 1 can be rewritten as in Xing et al. (2017):

$$FChla_{cor} = FChla_{meas} - Slope_{FDOM} * FDOM_{meas} - \alpha \tag{2}$$

$$\alpha = FChla_{dark} - Slope_{FDOM} * FDOM_{dark} \tag{3}$$

Equation 2 shows that $Slope_{FDOM}$ and α can be easily retrieved with a linear regression in the depth range where $FChla_{meas}$ is expected to be null due to the absence of Chla. This depth range starts at the Chla minimum down to the bottom depth of the profile, this water layer will be hereafter referred to as the deep layer while the layer above the Chla minimum will be referred to as the surface layer. Moreover, the MLD was always found above the depth of the Chla minimum making it easy to determine the regression interval used for the determination of both parameters. Once the latter are known, the profile can be corrected according to Equation 1. Similarly to Chla data, CDOM data were smoothed with a 5-point moving median filter in order to avoid potential spikes that could lead to a poor quality linear regression. However, no quality checks have been defined for CDOM at the moment (QC = 0).

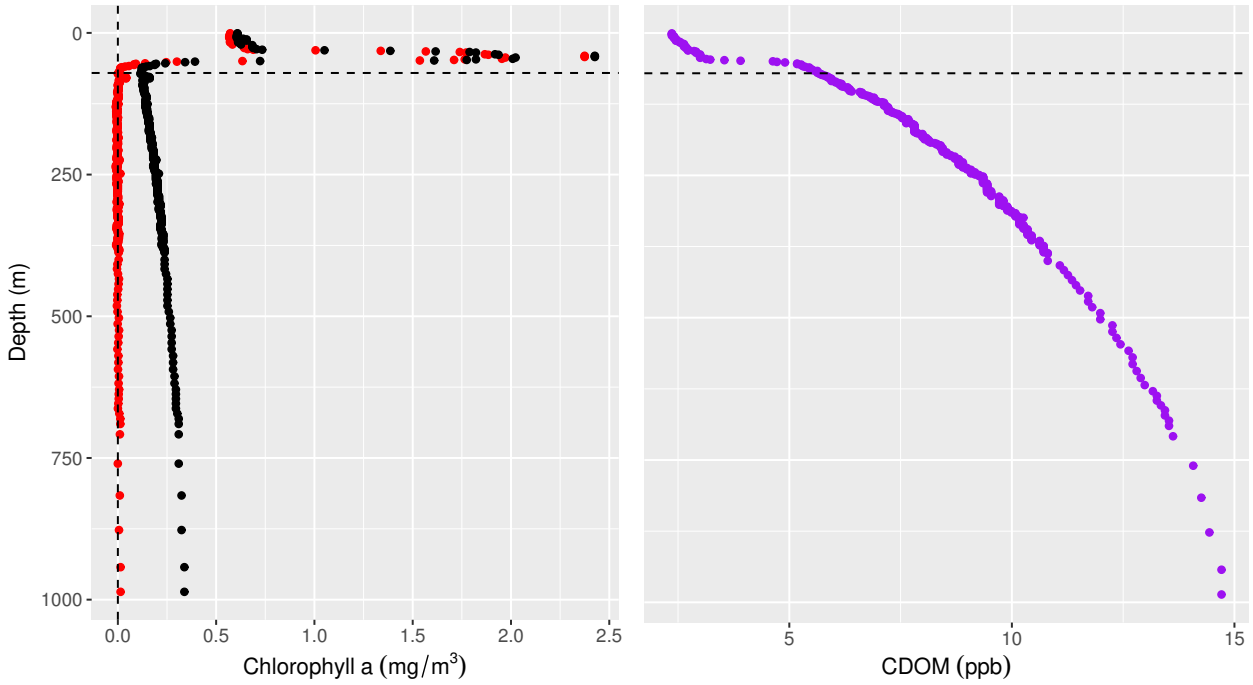

Figure 5: Chla (black) and CDOM (purple) measured by the float WMO 6900807 on the 30-03-2015. In red, the FDOM-based corrected Chla profile. The vertical and horizontal dashed lines represent the zero abscissa and the starting depth for the linear regression, respectively.

After that, a NPQ correction method was applied to all corrected Chla profiles (Fig. 6) otherwise false DCM (especially in the winter months, see for instance Fig. 7a) would have been retained due to this effect. Thus, the maximum chlorophyll (*i.e.* converted from fluorescence) value in the MLD, determined by finding the depth where the density gradient is above 0.03 kg m^{-3} compared to the surface density (de Boyer Montégut et al., 2004), is extrapolated to the surface (Schmechtig et al., 2014). The surface density was fixed at 10 m as in de Boyer Montégut et al. (2004). Though, the general criterion for the MLD in the Black Sea is usually a density gradient above 0.125 kg m^{-3} referenced at 3 m (Kara et al., 2009), it

could not be used here due to many potentially bad data close to the surface.

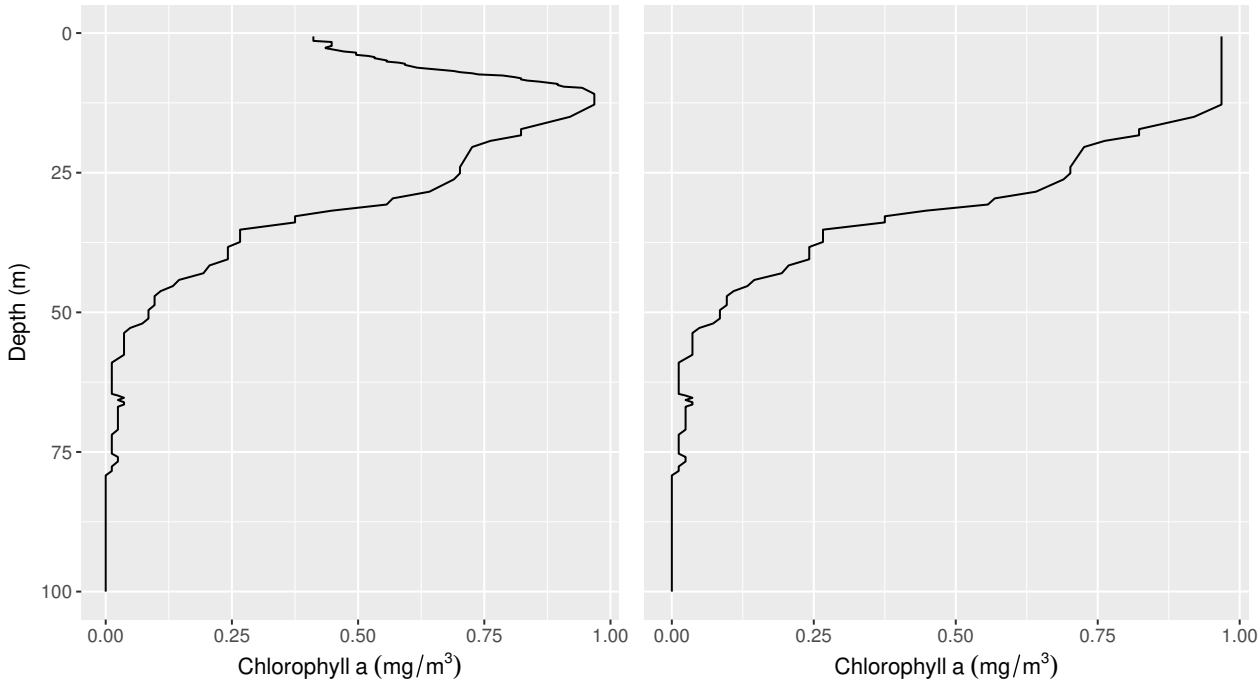

Figure 6: NPQ correction for the float WMO 7900592 on the 03-01-2014. Left and right figures: before and after NPQ correction.

Photosynthetically available radiation (PAR) profiles corresponding to the presence of a DCM in the water column (208 profiles) were visually inspected due to the lack of quality control (QC = 0). Four profiles had to be removed. Due to the scarcity of common depths for simultaneous measurements of both Chla fluorescence and PAR, the value of PAR at the DCM was interpolated at the depth of the DCM. Finally, a 5-point moving median filter was also applied to smooth the signal and to remove potential spikes (spotted in the visual analysis).

3.2.2 Data processing

Fluorescence profiles were firstly fitted to a Gaussian distribution and a sigmoid curve to discriminate, in a first approach, DCM-like profiles from homogeneous profiles where the Chla concentration is homogeneous in the mixed layer (*e.g.* Uitz et al., 2006). In place of the Gaussian distribution from Platt et al. (1988) used by Navarro and Ruiz (2013), it has been chosen to use the equation implemented by Mignot et al. (2011) to take into account the surface chlorophyll background, often exceeding by far bottom values. This procedure was applied to the first 100 m of the water column to avoid considering potential deep secondary Chla peak occurring at the interface with the sulfidic water layer associated with phototrophic bacteria (*e.g.* Coble et al., 1991). The first equation will then be referred as the Gaussian fit and the second as the sigmoid fit:

$$F(z) = F_{surf} e^{\frac{-ln2}{Z_{1/2}} z} + F_{max} e^{\frac{-(z-Z_{max})^2}{dz^2}} \tag{4}$$

$$F(z) = F_{surf} \frac{1}{1 + e^{(Z_{1/2}-z)s}} \tag{5}$$

F_{surf} is the fluorescence value at the surface, $Z_{1/2}$ the depth where F_{surf} is divided by 2, F_{max} the maximum value of the Gaussian fit, dz the proxy of the Gaussian fit thickness, Z_{max} the depth of the Gaussian fit maximum and s the proxy of the sigmoid fit slope at $Z_{1/2}$. Data were fitted using a nonlinear square fit function applying the Levenberg-Marquardt algorithm (Moré, 1978) implemented in (RStudio Team, 2016). It has been chosen to keep profiles where the unexplained variance between the raw profile (observations) and the fitted Gaussian curve was below 20%. We decided to use the threshold of 20% as in Mignot et al. (2011) instead of 10% used in Navarro and Ruiz (2013) because it appeared to be too restrictive. Rejected profiles were classified as "others" similarly to Mignot et al. (2011). Sigmoid-fitted profiles with a higher coefficient of determination r^2 (hence a lower unexplained variance) than Gaussian-fitted profiles were classified as "sigmoid" (see Fig. 8 for a summary of all kinds of profiles found in the Black Sea). The others were classified as "Gaussian". Results show 64,63% of Gaussian profiles (402 profiles), 32.96% of sigmoid profiles and 2.41% of other profiles. As observed by Mignot et al. (2011) in the Mediterranean Sea, profiles characterized as "others" were partially due to the presence of double fluorescence peaks. Similarly to Navarro and Ruiz (2013), profiles with a DCM below 1 m were also removed (6 profiles removed). After visual inspection of our database (396 profiles left), DCM-like (pseudo-Gaussian) profiles can be split into 3 categories based on Lavigne et al. (2015) : DCM, modified DCM, high surface chlorophyll (HSC) (see Fig. 7b). Homogeneous and complex (odd) profiles were, in principle, removed at the previous step because they were classified as, respectively, "sigmoid" and "others" profiles. In this study, only DCM and modified DCM will be investigated. As such, profiles will be classified as HSC if the mean fluorescence value over layers 10 m wide is strictly decreasing (Lavigne et al., 2015). However, small variations can still occur in the deep layer even after the FDOM-based correction potentially allowing the non-discrimination of all HSC profiles. Consequently, this algorithm will be applied from the surface to the depth of the fluorescence minimum rounded up to the nearest ten. On the other hand, profiles will be classified as DCM if F_{max} is at least twice as large as F_{surf} (Lavigne et al., 2015) and as modified DCM if not. Nevertheless, due to the uncertainty of the criterion for modified DCM profiles, a visual inspection was performed and a new criteria arose: profiles for which the fluorescence maximum accounts for less that 90% of the value at the surface are classified as "undetermined". Profiles belonging to this category could potentially be the very beginning or the very ending of a DCM because they only occur at either the end or the start of the year, mainly in the winter months (Fig. 7b). Globally, 56 profiles were classified as "HSC", 237 as "DCM", 80 as "modified DCM" and 23 as "undetermined". Consequently, this study will retain only the two latter categories hence 317 profiles which represent $\approx$ 37.5% of our initial database.

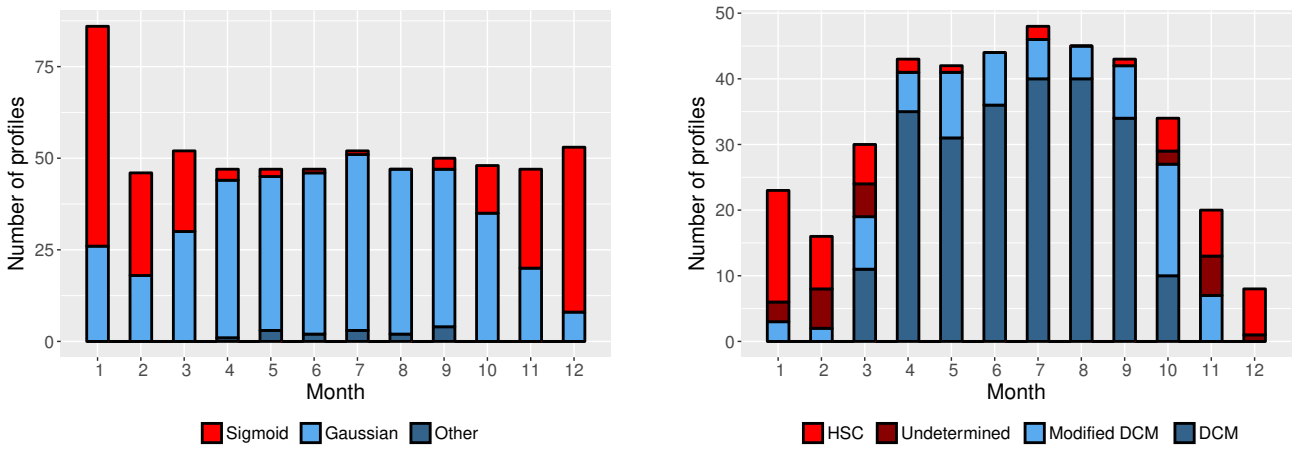

(a) (b)

Figure 7: Histograms of (a) all profiles (622) after fitting (b) pseudo-Gaussian profiles.

Finally, in order to get the s_θ associated to the DCM or modified DCM where the depth is now known thanks to the fitting process, each variable (Chla, temperature and salinity) is gathered for each common depth, then the closest value to the depth of the DCM/modified DCM is taken and the potential density is computed. No instrumental drift was noticed in the data. All these information will then be written in a text file used by *DIVAnd* for further analyses. A toolbox for automatic creation of input files for *DIVAnd* from Argo floats data is currently under development (see Annexes for more information).

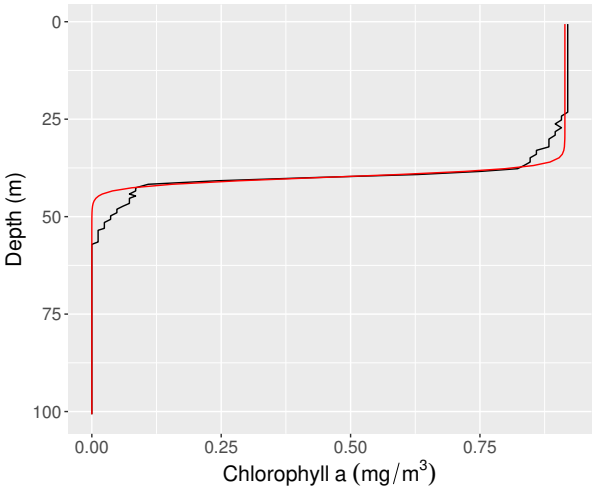

(a) Homogeneous

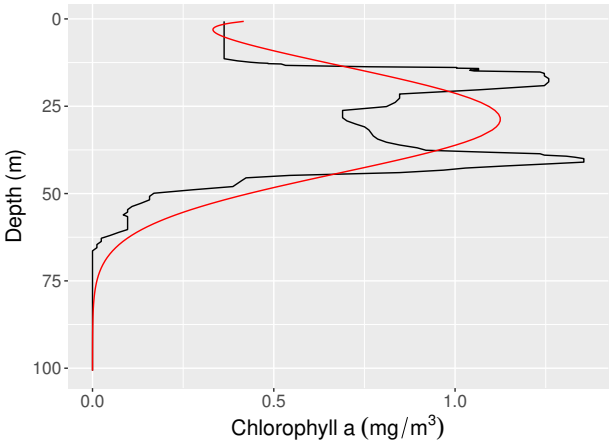

(b) Complex

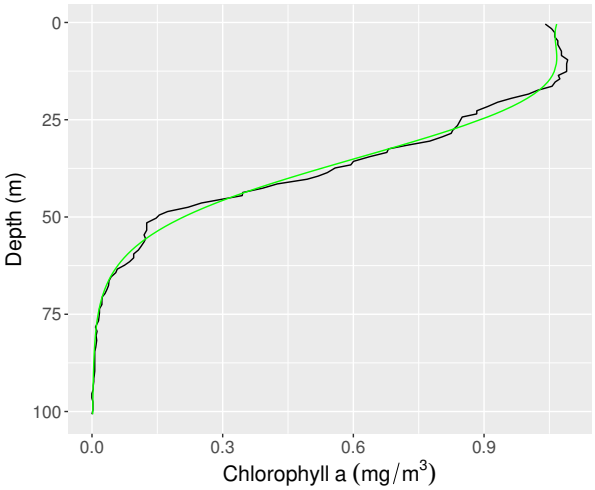

(c) HSC

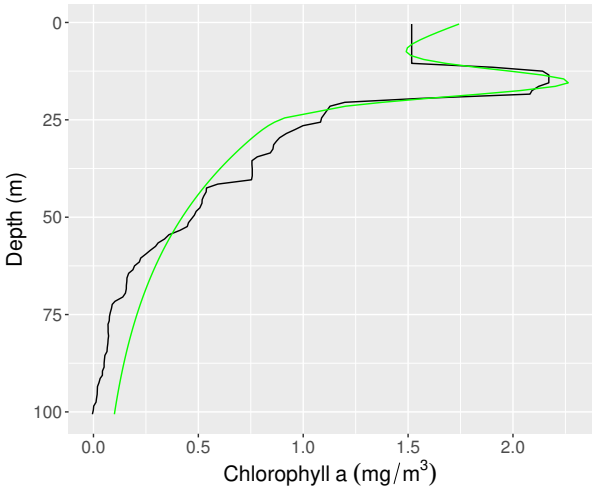

(d) Modified DCM

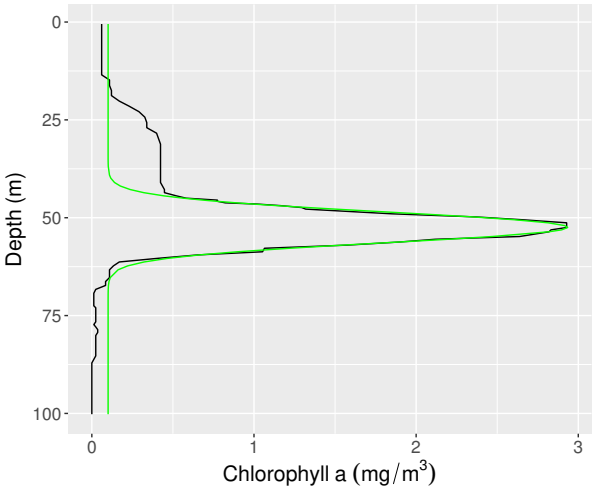

(e) DCM

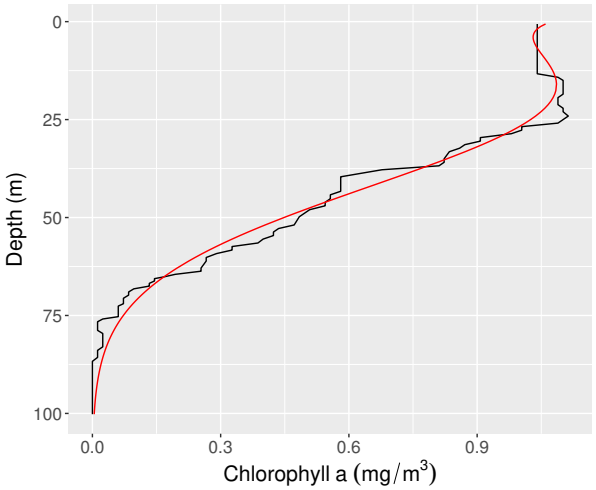

(f) Uncertain

Figure 8: Different flavours of profiles encountered in the Black Sea. All profiles are fitted with Equation 4 except (a) which is fitted with the sigmoid (Equation 5).

3.2.3 DIVAnd software

In order to investigate the spatial distribution of the DCM, we will use the *DIVAnd* analysis tool (Barth et al., 2014) to interpolate discrete observations of DCM and derive continuous fields from it. *DIVAnd* is a software developed at the University of Liège (GHER group). It is in some way the new version of *DIVA*, *i.e.* Data Interpolating Variational Analysis (*e.g.* Troupin et al., 2013), except that it now allows n-dimensional variational data analyses, *i.e.* it can work in any n-dimensional space. From a set of inhomogeneously distributed discrete observations, *DIVAnd* is able to derive a continuous field that fulfills mathematical constraints over the domain of study (Troupin et al., 2012). The latter are expressed in the form of a cost function composed, in our study, of two terms: the observation constraint which represents the misfit between observations and analysis and the smoothness constraint to avoid strong gradients (among others). The fact that *DIVAnd* does not strictly interpolate observations comes from inherent errors (noise) particularly present in oceanographic data such as instrumental errors, representativeness errors and synopticity errors (Rixen and Beckers, 2002). In this study, *DIVAnd* is used to map the spatial distribution of the DCM with depth and density from March to October, where we expect to have a DCM (Fig. 7b).

3.2.4 Mathematical formulation

Considering a series of N data d_i at locations $\mathbf{x}_i$, a cost function J is defined (Barth et al., 2014):

$$J[\phi] = \sum_{i=1}^{N} \mu_i [d_i - \phi(\mathbf{x}_i)]^2 + \|\phi - \phi_b\|^2 + J_c(\phi) \tag{6}$$

where μ_i is the weight of the observations, ϕ_b is the background field (which will be further discussed) and $J_c(\phi)$ is the additional constraints (*e.g.* advection constraint) term. The latter will not be used and can therefore be considered to be zero. The first term is the observation constraint while the second term represents the smoothness constraint which is a measure of the spatial variability of the analyzed field (curvature, gradient and value). Using Equation 6 (see details in Barth et al., 2014), we introduce L, a characteristic length scale further denoted as correlation length and λ, the signal-to-noise ratio. The correlation length quantifies the influence distance of a data to its neighbours while λ measures the confidence in the data (Troupin et al., 2012).

3.2.5 Background and parameters determination

In this study, the background field is an averaged field used to compensate lacking data. As a result, we need to define a meaningful spatial averaged field. The depth and density distributions of the DCM over the years (Fig. 9) show that the spatial variability is greater than the seasonal variability thus we consider essential that the background field retains the spatial variability rather than the seasonal one. In order to estimate this background, we realize a coarse interpolation of the depth and the density of DCM with *DIVAnd*. To this aim, we firstly calculated the anomalies of both variables (depth and density) for observations between March until October, where a DCM is expected, compared to an averaged value computed over all data (ignoring seasons and years of collection). Then, the calibration of the two parameters L and λ is done

manually in the sense that it is based on a visual screening[1] of several outputs regarding different sets of parameters. The objective is to find a relatively smooth resulting analysis which will then be used as the new background for further analyses. The set of parameters allowing such a field was chosen to be L = 5° (arc degree) and λ = 2. Then, based on the histogram (Fig. 7b), three periods (pseudo-seasonal periods) were defined for refined analyses: the DCM formation period from March to April, the summer period (DCM well defined) from May to July and the DCM ending period from August to October. For each period, the correlation length was evaluated statistically by fitting the theoretical kernel (second term of Equation 6) to the correlation between data, however the maximum L value from all periods was 0.115 arc degree which only represents approximately 8 km. Those correlation lengths were considered to be too small to bring out exploitable results, hence it has been chosen to use realistic L (and λ) giving tangible results.

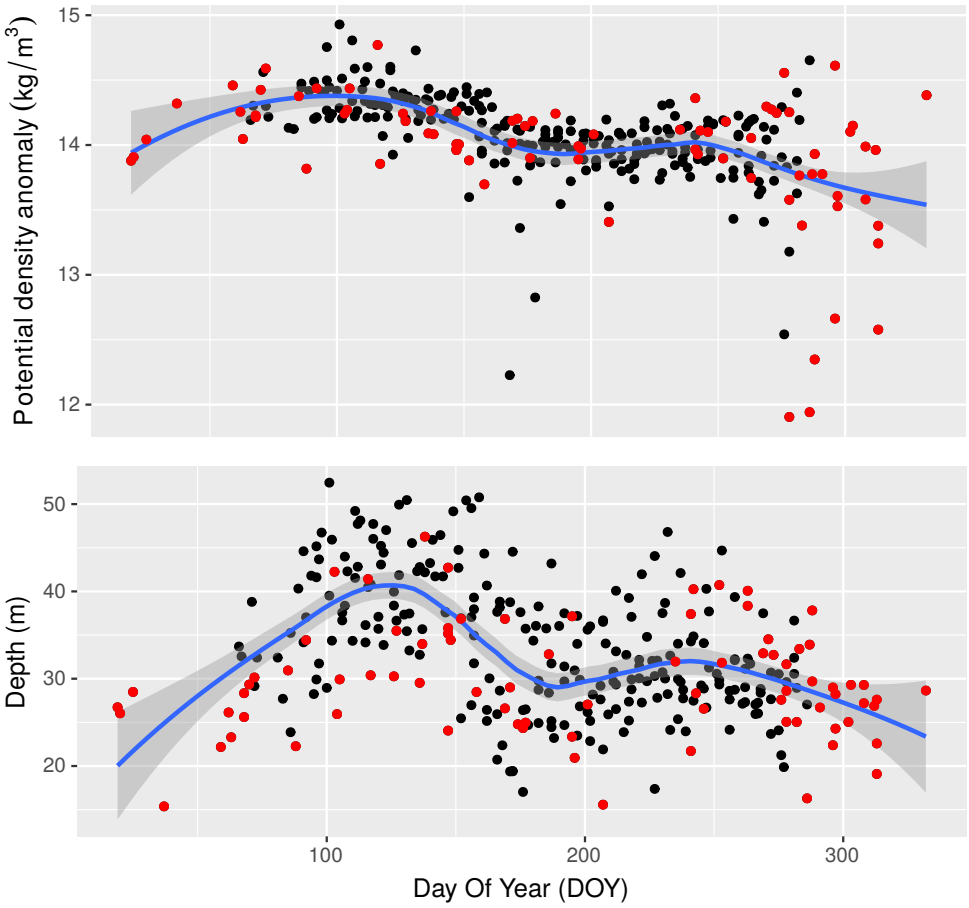

Figure 9: Distribution of DCM (black) and modified DCM (red) according to the Day Of Year (DOY) for the period 2014-2017. The blue line represents the smoothed (loess smoother, span = 0.5) DOY series considering all years. The shaded area depicts the 95% confidence interval.

[1]A screening is defined here as the output of several *DIVAnd* analyses performed with multiple combinations of L and λ, awaiting visual study from the user.

3.3 Validation data

3.3.1 Chla sampling

In order to evaluate the empirical equation proposed by Xing et al. (2017) for retrieving Chla from fluorescence data impacted by CDOM, we compare HPLC-derived Chla (considered as the most accurate estimation of Chla (Dos Santos et al., 2003)) with Chla estimated from BGC-Argo floats using the FDOM-based method of Xing et al. (2017).

Sampling took place on the 29th of March 2018 at a station localized at 43°10'N and 29°E in the Black Sea (Fig. 4). Seawater samples were obtained using a CTD carousel equipped with twelve 5-L Niskin bottles. Samples were taken at 12 different depths between 1000 meters and the surface, and were considered to be co-located in time and space with the float deployment similarly to Taillandier et al. (2018). After that, seawater samples were vacuum filtered through 47mm diameter Whatman GF/F glass fibre filters (0.7 μm pore size). This procedure, along with the collection of discrete water samples further analysed with HPLC is the validation method widely accepted by the community (Roesler et al., 2017). No bloom or strong DCM was present during that period, filtered volumes varied between 4L near the surface and approximately 5L between 100m and 1000m. After filtration, filters were immediately stored in liquid nitrogen and then at -80°C until HPLC analyses. These analyses were performed using the procedure from Ras et al. (2008) for the determination of Chla concentration and other pigments.

3.3.2 Deployment data

This float (WMO 6903240) was deployed in the Black Sea by the R/V Akademik on the 29th of March 2018. The first Chla profile taken after deployment (during the descent) will be referred to as the validation profile in the rest of the manuscript. Data acquired by the float were not immediately transmitted to the Coriolis data center hence those raw data - not quality controlled - were provided by the Oceanographic Laboratory of Villefranche-sur-Mer (France). These data are not publicly available yet but they should be available on Coriolis soon (*ftp://ftp.ifremer.fr/ifremer/argo/dac/coriolis/*). Consequently, Chla and CDOM data were quality controlled using Schmechtig et al. (2014). First of all, $FDOM_{meas}$ and $FChla_{meas}$ data (in counts) were converted to conventional units (ppb and mg m^{-3}, respectively) using the dark and scale factors provided by the manufacturer with:

$$Chla = (FChla_{meas} - FChla_{dark}) * Scale_{Chla} \tag{7}$$

$$CDOM = (FDOM_{meas} - FDOM_{dark}) * Scale_{CDOM} \tag{8}$$

Then, spikes were removed, data found at the same depth were averaged and both signals were smoothed with a 5-point moving median filter to reduce the background noise. In a recent paper (Roesler et al., 2017), it has been shown that in addition to NPQ (Xing et al., 2012a) and CDOM corrections (Xing et al., 2017), there was still an extra bias coming from the factory-provided calibration for *WET Labs ECO* series chlorophyll fluorometers. Each float in this study is equipped with such a sensor. Their paper suggests that Chla fluorescence measured by this brand of fluorometers is globally overestimated by a factor of two except in the Black Sea where they found a factor below 1 (0.7). The latter is considered as an underestimation of

the unknown real factor and would be the consequence of the particular relationship between fluorescence and irradiance - through the diffuse attenuation for downward irradiance -, in waters with a significant CDOM reservoir (Xing et al., 2011; Roesler et al., 2017). We will not apply such a correction factor because we consider that it still remains uncertain in the Black Sea. Moreover, it will have strictly no impact on our results but this bias will need to be taken into account for further studies focusing on Chla concentrations.

3.4 Implementation of a new correction method

Based on the regularity of CDOM profiles (both in space and time, see Fig. 10), a new approach has been thought in order to correct Chla profiles from floats lacking CDOM fluorometers. The different calibration of the CDOM fluorometers is obvious (Fig. 10), however Chla fluorometers measured roughly, at least at depth, the same values (not shown).

Globally, the CDOM profiles delivered by the two BGC-Argo floats (WMO 6900807 and 6901866) exhibit low spatial and temporal variability in terms of vertical shape and absolute values, considering the calibration difference. Therefore, based on their shape, *i.e.* relatively uniform at the scale of the basin, it has been chosen to create a typical CDOM profile. By doing so, we make the hypothesis that the shape of the profile is much more important than its absolute values. Several approaches are possible for the creation of such a representative - albeit virtual - CDOM profile but our study will not be very exhaustive. In our opinion, the most blunt approach would consist in taking the mean of true CDOM profiles from both floats but, after some tests, we observed that the shape is diverging at depth, probably due to the sampling scheme (see gaps at depth in Fig. 10) and our bin average process (see further explanations below). Nevertheless, good results were already obtained using this - not perfect - mean profile. In order to get rid of the variations at depth (noisy corrections) and based on our hypothesis, we decided to create a virtual CDOM profile from the mean of all CDOM profiles taken by only one float (WMO 6900807), *i.e.* 212 profiles. This profile is the result of the mean of all CDOM profiles that were previously binned differently according to the definition of three layers. The latter have been thought to match the logic of the vertical sampling scheme of an Argo float, *i.e.* a decrease in the sampling frequency with depth. As a result, it has been chosen to bin real CDOM profiles every 1 m, 5 m and 10 m for regions located between, respectively, 0 and 200 m, 200 and 400 m and finally below 400 m. This choice is not random but it could be further improved with a specific "bin scheme" according to the precise vertical sampling scheme programmed in each float endowed with a CDOM sensor (Argo Data Management Team, 2017). The method consists in applying the FDOM-based method except that the CDOM profile is now the virtual CDOM profile interpolated on each depth of the Chla profile.

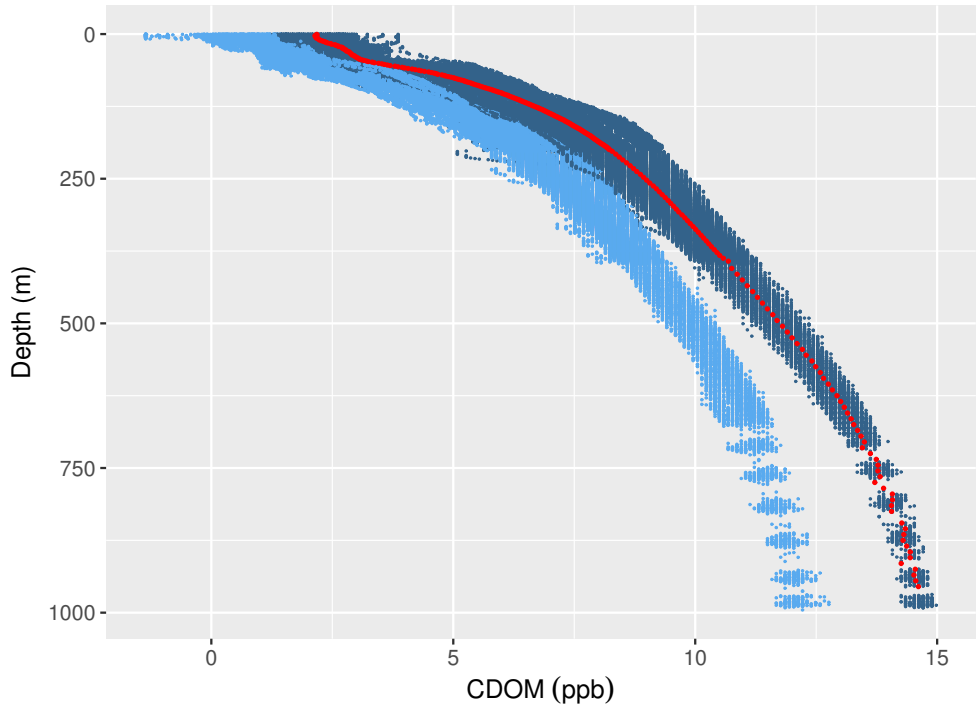

Figure 10: CDOM profiles obtained by BGC-Argo floats WMO 6900807 (dark blue) and 6901866. In red, the mean CDOM profile.

To validate our approach, we will apply the correction based on the virtual CDOM profile on Chla profiles from the float 6901866 that were corrected with their respective (real) CDOM profiles. After that, we will test our virtual profile on a new data set, *i.e.* the two floats lacking CDOM fluorometers (WMO 7900591 and 7900592).

3.5 Types of Chla profiles correction

In the rest of this manuscript, several types of correction will be used on Chla profiles and will be referred to the different types described in Table 1 below:

Type	Meaning
Uncorrected	No correction has been applied on the profile
FDOM-based	Chla profile corrected with the FDOM-based method (Equation 1), *i.e.* correction of the influence of CDOM on Chla fluorescence
QFDOM-based	FDOM-based profile with NPQ correction at the surface
MFDOM-based	Chla profile corrected with the FDOM-based method applied with slope$_{FDOM}$ and α averaged on 404 profiles (Chla and CDOM) taken by two floats (WMO 6900807 and 6901866) for the period 2014-2017
VFDOM-based	Chla profile corrected with the FDOM-based method used with a virtual CDOM profile

Table 1: Summary of the different types of correction used on Chla profiles.

4 Results

4.1 Estimation of Chla from fluorescence

4.1.1 The FDOM-based method

The HPLC analysis (Fig. 11) shows that below a depth of 140 m, there is no more Chla. Hence, the increase in the Chla signal measured by fluorometers mounted on Argo floats in the Black Sea is not associated to Chla but more likely results from the presence of high levels of CDOM. Above 50 m, the HPLC analysis shows a negligible maximum (0.611 mg m^{-3} at the surface and 0.643 mg m^{-3} at 30 m) although more samples would have been needed to demonstrate the presence or absence of a subsurface chlorophyll maximum as indicated by the net peak in the fluorescence profile at approximately 25 m. On top of that, the minimum in fluorescence (hence Chla) measured by the float (Fig. 11, black curve) is located at 94.3 m (0.095 mg m^{-3}) while the minimum non negligible value from discrete water samples is located at 140 m (0.012 mg m^{-3}). Below, Chla concentrations measured by HPLC are very low, ranging from 0.002 to 0.004 mg m^{-3}, and can thus be considered as null.

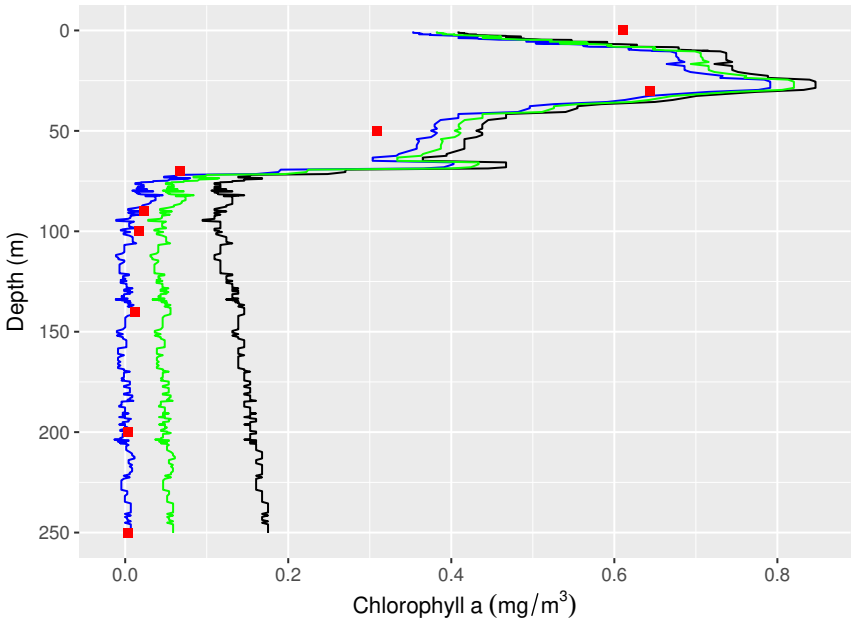

Figure 11: Application of corrections (MFDOM-based (green) and FDOM-based (blue)) on the validation profile (black). Red squares depict discrete samples determined with HPLC.

Results show that on average, in the Black Sea, slope_{FDOM} equals 0.026 $\pm$ 0.001 mg m^{-3} ppb^{-1} and α equals -0.020 $\pm$ 0.015 mg m^{-3}, which is consistent with the values found by Xing et al. (2017) for the Black Sea. On the other hand, it can clearly be seen (Fig. 11) that the FDOM-based method applied on the validation profile is coherent with HPLC data. In the surface layer, the RMSE[2] between Chla estimations obtained by HPLC (observations) and Chla retrieved from the validation profile corrected with the FDOM-based method (modeled values) is equal to 0.144 mg m^{-3}. Below, the RMSE is equal to 0.008 mg m^{-3}. For the uncorrected profile (black), the RMSE is equal to 0.169 and 0.143 mg m^{-3} for, respectively, the surface

[2] $\sqrt{\frac{\sum_{n=1}^{N}(obs_n - mod_n)^2}{N}}$ where obs are observations, mod are modeled values and N is the number of points.

and deep layers. In the surface layer, uncorrected and FDOM-based corrected profiles show similar RMSE. This is probably because CDOM concentrations are low in this layer, potentially because CDOM encounters photochemical (photodegradation) effects under the action of light (Xing et al., 2012b). Furthermore, we are rather confident that the FDOM-based correction is a valid method to retrieve consistent Chla values in the Black Sea. Indeed, when comparing different correction methods (Table 2), we obtain the lowest RMSE value (after NPQ correction) for the entire FDOM-based Chla profile. In the deep layer, this profile is well adjusted to zero (Fig. 11) and the RMSE of 0.008 mg m^{-3} can be considered as a significant improvement compared to the uncorrected and MFDOM-based (0.044 mg m^{-3}) Chla profiles.

Correction	slope$_{FDOM}$	α	RMSE (mg m^{-3})
None	—	—	0.158
FDOM-based	0.033	-0.004	0.107
MFDOM-based	0.026	-0.021	0.116
QFDOM-based	0.033	-0.004	0.088

Table 2: RMSE for different corrections (with regression coefficients, slope$_{FDOM}$ and α) applied on the validation profile.

4.1.2 The VFDOM-based method

For 192 profiles (WMO 6901866), the RMSE was computed between the FDOM-based (observations) and the VFDOM-based (modeled values) Chla profiles (Fig. 12). On average, we found a RMSE of 0.009 $\pm$ 0.005 mg m^{-3} with a minimum and maximum value of 0.003 and 0.0285 mg m^{-3}, respectively. Averages and standard deviations (Sd) for regression parameters obtained with all profiles are resumed in Table 3 below:

Correction	Mean slope$_{FDOM}$	Sd slope$_{FDOM}$	Mean α	Sd α
FDOM-based	0.027	0.001	-0.008	0.010
VFDOM-based	0.025	0.002	-0.03	0.022

Table 3: Comparison between FDOM and VFDOM-based methods for 192 profiles.

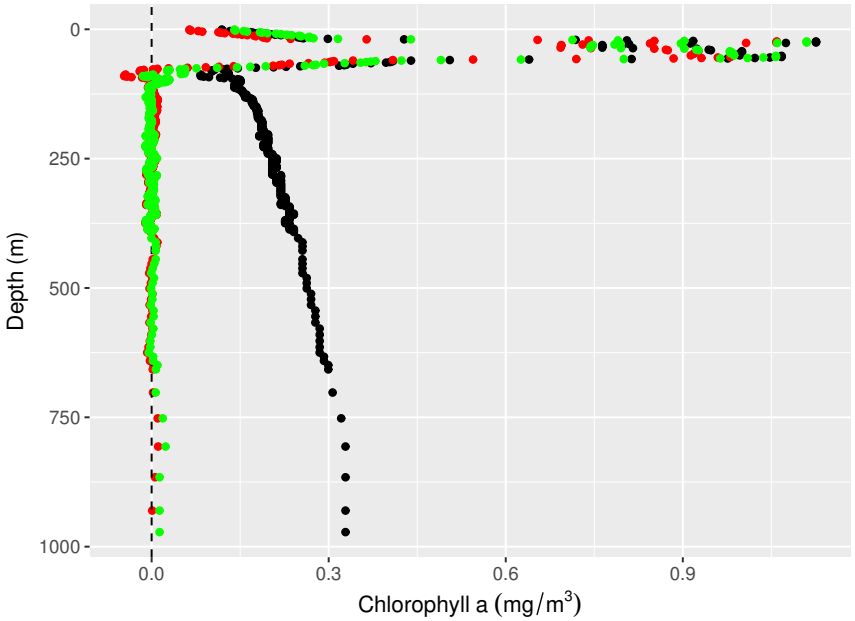

Figure 12: Uncorrected (black), FDOM-based (green) and VFDOM-based (red) Chla profiles. This graph represents the case where the RMSE between FDOM and VFDOM-based methods is maximum, *i.e.* 0.0285 mg m^{-3}.

Results clearly show that, at least at depth where we observe the monotonous increase in fluorescence, the VFDOM-based method is rather accurate and that the shape seems to be the most important factor for the correction. If we now look at the new float (WMO 6903240), we can also try to validate this method with the HPLC profile. Again the RMSE between both FDOM and VFDOM-based corrections is very low (0.007 mg m^{-3}) whereas absolute CDOM values differ greatly (means of 3.75 ppb for the true profile versus 6.13 ppb for the virtual profile). As for the HPLC profile, it is even better (see Table 2) with a RMSE of 0.102 mg m^{-3}.

We are aware that many other representative CDOM profiles could have been implemented and may even lead to better results. For instance, we could have implemented a seasonal or an annual profile to take into account potential temporal differences in CDOM profiles across the basin. Similarly, we could also have defined several spatially-limited (zonal) profiles to consider spatial variations of CDOM concentrations over the Black Sea (*e.g.* west and east basin), although none have been noticed in our preliminary study (see also, Fig. 10). Nevertheless, our findings show a great confidence in this first approach and that the idea of a mean profile is not so far-fetched.

After the application of the VFDOM method, a visual inspection was performed on all profiles (270) from BGC-Argo floats WMO 7900591 and 7900592. Even if the correction cannot be quantified, it is clear that results are rather satisfactory because we can see a significant improvement of Chla profiles, especially at depth (Fig. 13). In our opinion, the VFDOM-based correction is valid for every single profile, except when first data available from Chla profiles start at a depth surprisingly deep (for instance below 100 meters) and "depth-stuck" profiles, *i.e.* abnormal profiles obtained from BGC floats. The latter could have been spotted with a quality check prior to the correction but show at least that the issue did not come from the VFDOM method.

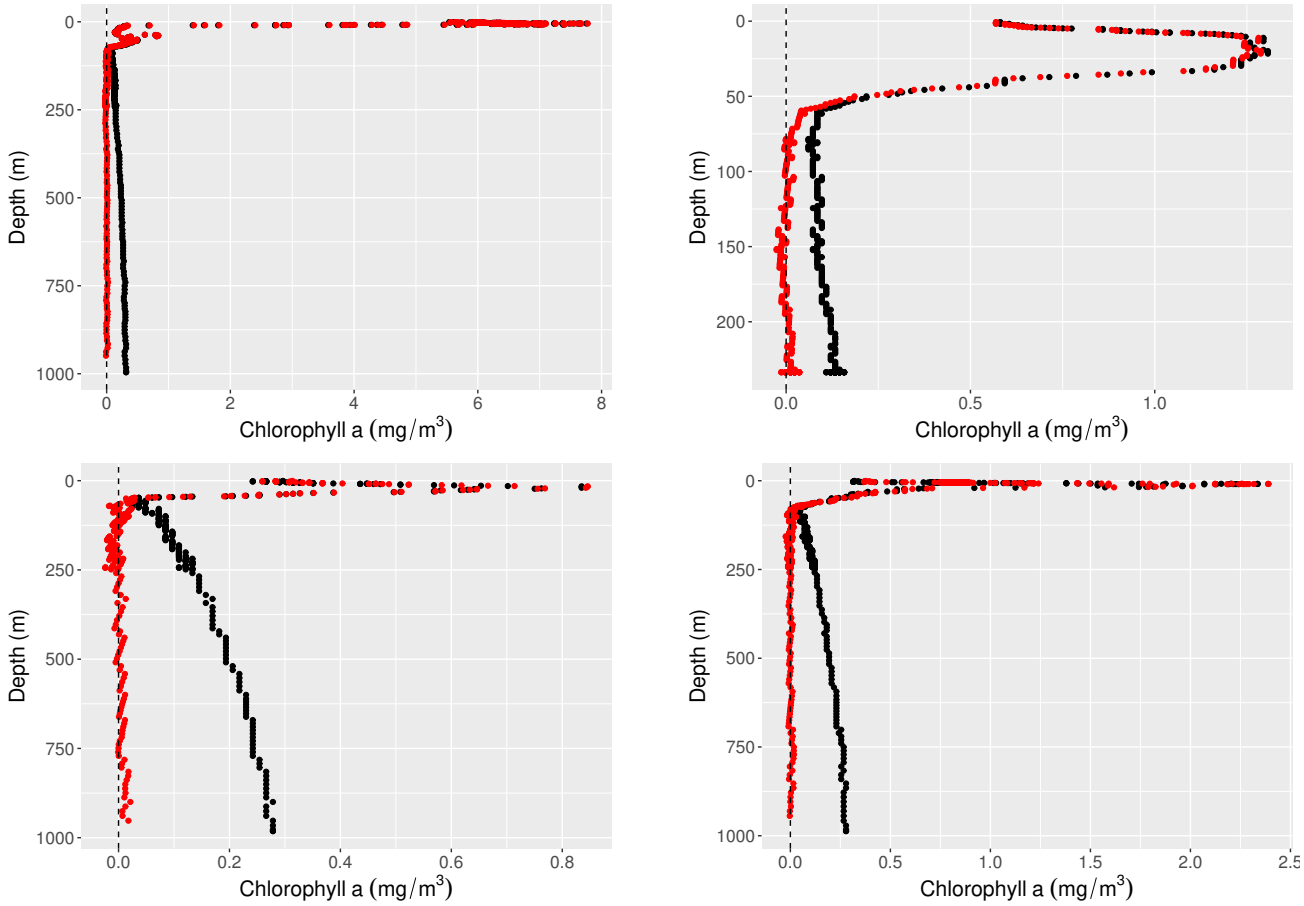

Figure 13: Examples of corrected profiles (red) for floats WMO 7900591 and 7900592.

4.2 Analysis of DCM from corrected Chla profiles

Using now the most accurate estimations of Chla derived from the four BGC-Argo floats, we can therefore analyze the position of the DCM (with depth and density). As such, we will test the hypothesis of hysteresis proposed by Navarro and Ruiz (2013) and with that aim we will link the density of the DCM to that of the maximum MLD (hereafter referred to as density @max MLD). Table 4 shows trends for the MLD as well as the mean σ_θ found at the surface for each month from March 2005 to May 2018. It highlights the fact that the MLD can be considered as being maximum in January-February with a first approximation of the density @max MLD.

Month	Mean MLD (m)	Sd MLD (m)	Max MLD (m)	Mean $\sigma_{\theta-s}$ (kg m^{-3})	No. of profiles
January	35.47	13.96	89.6	13.98	418
February	32.57	16.82	138.3	14.11	349
March	22.65	11.54	68	14.09	389
April	15.90	8.73	53	13.85	362
May	9.99	2.40	23	13.22	338
June	9.39	1.55	18	12.17	298
July	9.66	2.19	19.6	11.20	310
August	10.59	3.02	23.4	10.64	282
September	13.43	4.71	29.9	11.11	319
October	16.75	6.55	41	12.28	359
November	21.54	9.08	52.8	13.07	349
December	31.85	12.77	79.5	13.67	405

Table 4: Summary of MLD statistics for each month covering the Black Sea between the 14-03-2005 and the 01-05-2018 (4178 profiles). Max: Maximum; Sd: Standard deviation; $\sigma_{\theta-s}$: surface potential density anomaly.

All years put together, DCM range between 15.38 m - 52.45 m and 11.90 - 14.93 kg m^{-3} (Fig. 18 and 21) while the potential density anomaly computed for January and February (months where the MLD appears to be maximal, cfr. Table 4) varies between 13.39 and 14.68 kg m^{-3}. The general pattern for the Chla maximum seems to converge at the σ_θ of the winter mixed layer (Fig. 14), although it is less obvious than results found in other temperate regions by Navarro and Ruiz (2013).

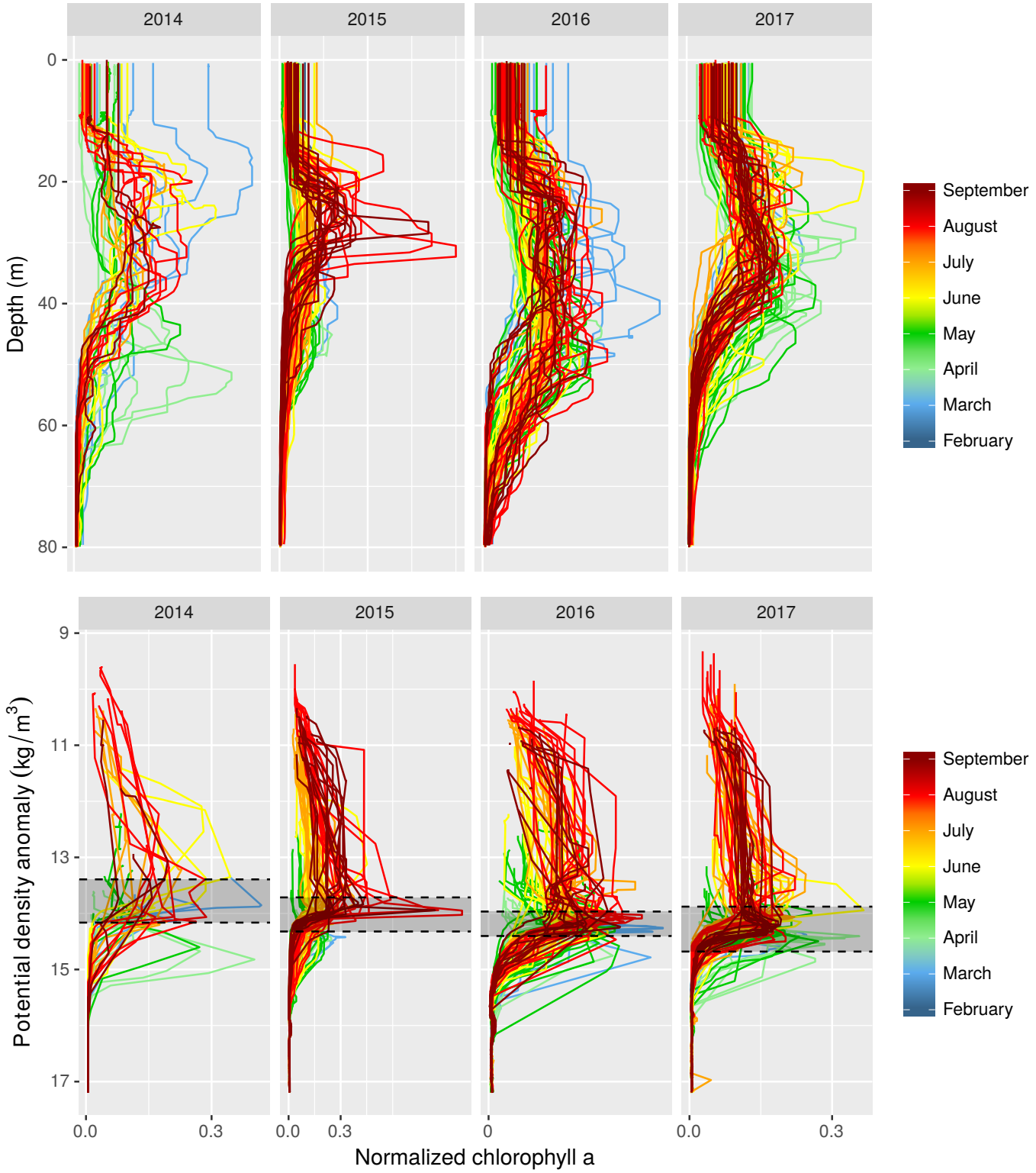

Figure 14: Interannual variability in Chla profiles. Top and bottom figures depict Chla versus depth and σ_θ, respectively. The grey area represents the range of σ_θ values measured by the four BGC-Argo floats in January and February where the MLD appears to be maximum (see Table 4). Chla data have been normalized [3] by taking into account all DCM and modified DCM profiles (317 profiles).

[3] $Chla_{normalized} = \frac{Chla - Chla_{min}}{Chla_{max} - Chla_{min}}$ for the DCM and modified DCM period (January to November).

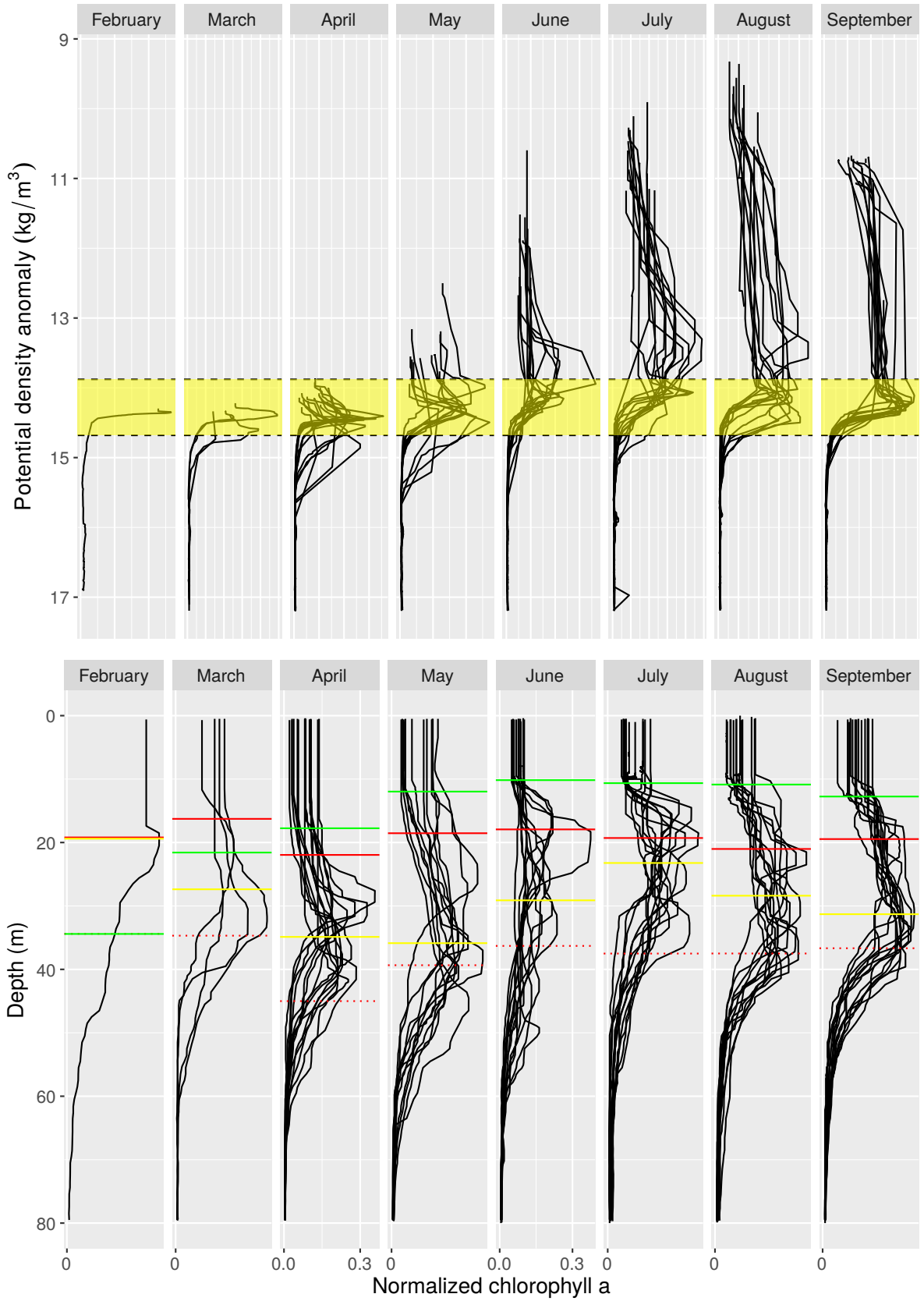

Figure 15: Evolution of the DCM in the basin of the Black Sea in 2017 estimated from Argo floats. Normalized Chla (see previous figure) profiles are plotted versus σ_θ (top) and versus depth (bottom). The yellow shading shows the range of σ_θ encountered in the mixed layer in January and February where it appears to be maximum. Mean depths of the 10% and 1% isolumes associated to DCM/modified DCM when available (204 profiles instead of 317) and mean MLD are represented by solid and dashed red horizontal lines and green line, respectively. Yellow horizontal lines represent the mean depth of the DCM for each month.

In 2017, the evolution of several DCM positions (Fig. 15) seems to corroborate the fact that its vertical variability is, again, mostly constrained by the density @max MLD ($\sigma_{MLD-MAX}$). Furthermore, the mean depth of monthly DCM is always located between the mean depths of both 1% and 10% isolumes [4]and always below the MLD (except in February) during the February-September period.

Once we look at the ratio between σ_{DCM} and $\sigma_{MLD-MAX}$ (Fig. 16), we notice that a vast majority lies between 0.95 and 1.05 with a mean value of ≈ 0.98. Nevertheless, Navarro and Ruiz (2013) found a highly pronounced peak at 1 in temperate latitudes (30°N - 45°N and 30°S - 45°S). A first explanation to this discrepancy albeit not so significant could come from the fact that σ_θ were computed using data from floats, hence the ideal condition would have been to get data from the specific water mass when a winter bloom occurred to get the most accurate value of σ_θ. This last condition is not necessarily met with BGC-Argo floats. Moreover, the global picture showing a ratio below 1 is plausible with an underestimation of the σ_θ from the water mass where the bloom occurred.

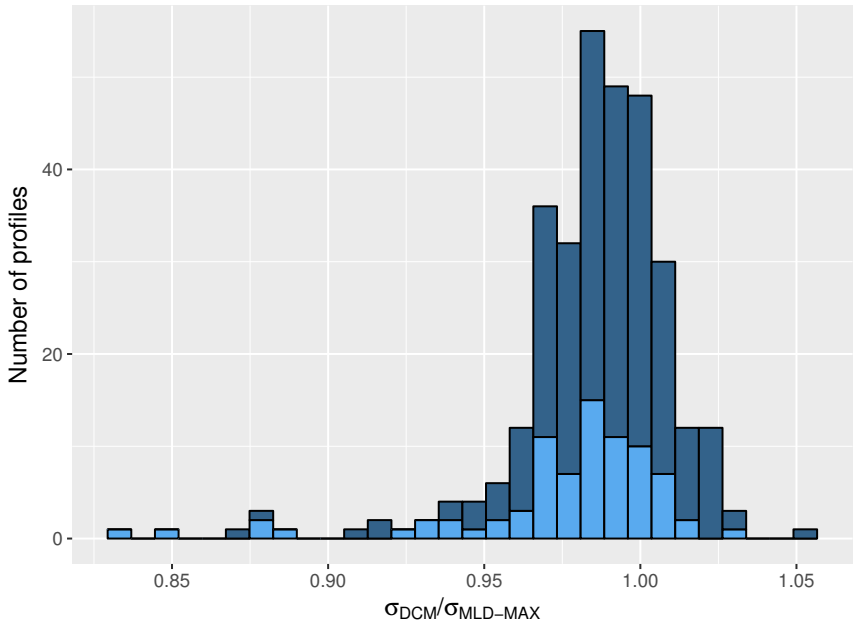

Figure 16: Histogram of density anomaly ratios. Dark blue and light blue represent DCM and modified DCM, respectively.

Spatially, this ratio seems to be very close to 1 (Fig. 17) in the center of the basin and in the western/eastern parts. In the west cyclonic gyre, it reaches the value of 0.975 and is globally near 0.96 and 0.975 in the east cyclonic gyre region. At first sight, contours match quite well mesoscale and submesoscale eddies pictured in Fig. 1.

[4]In February, the MLD and isolume 1% are mixed up at 34.4 m

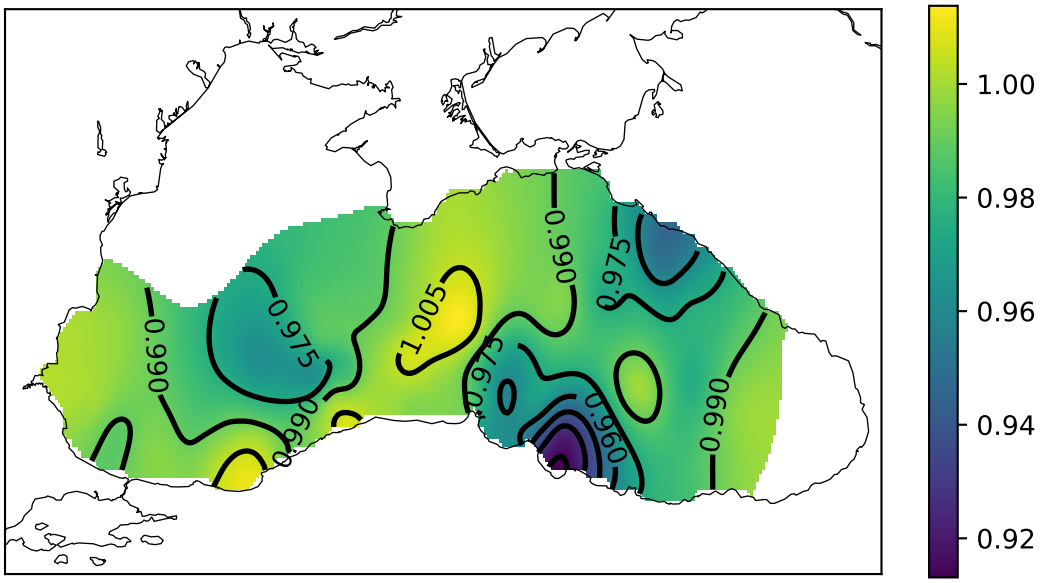

Figure 17: Map of the $\sigma_{DCM}/\sigma_{MLD-MAX}$ ratio (2014-2017) using *DIVAnd* with parameters (L, λ) = (1°, 2). White zones represent areas where the error field after analysis is beyond 50%.

4.3 Spatio-temporal analyses of the DCM

4.3.1 Depth analysis

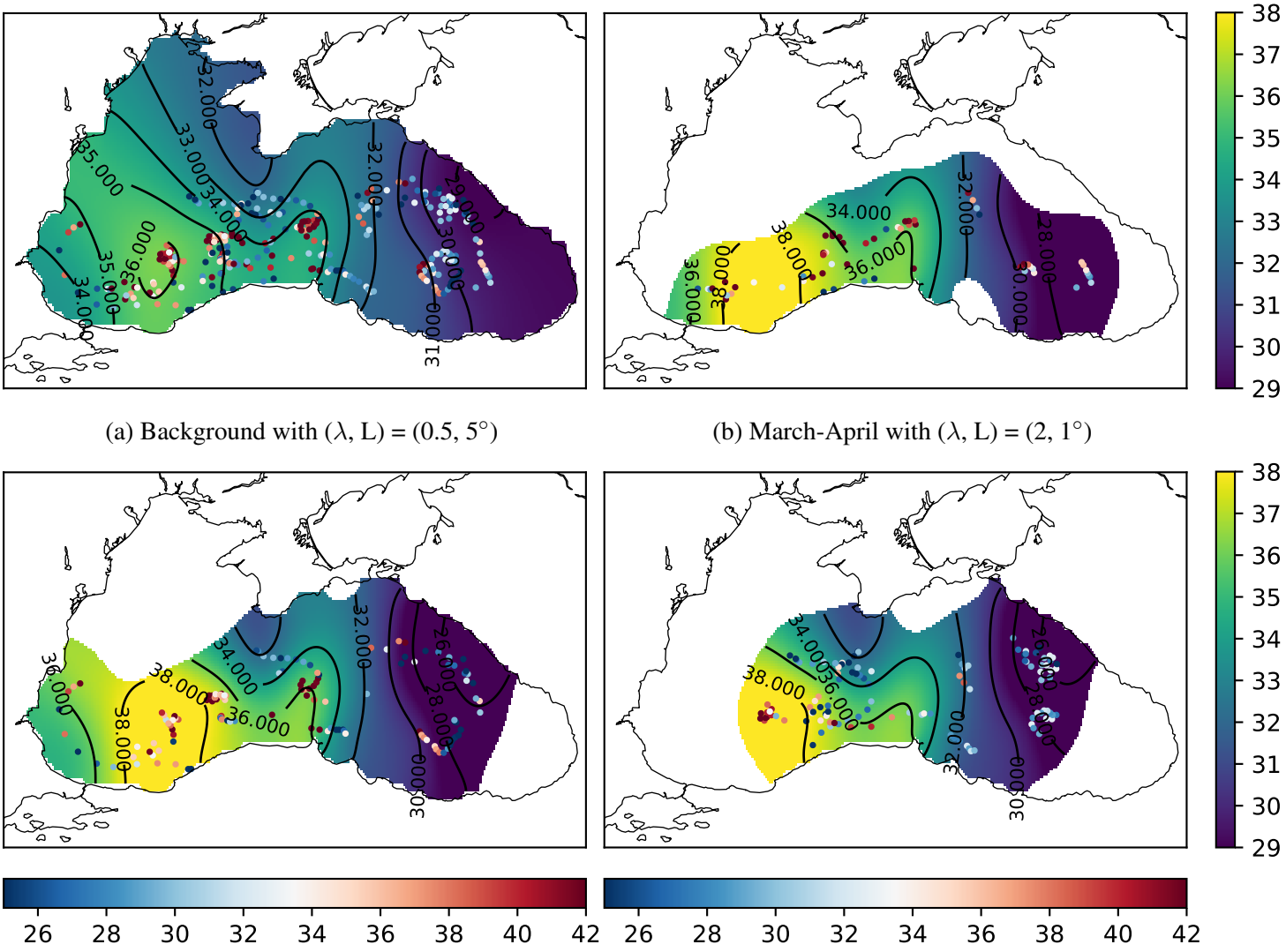

(a) Background with (λ, L) = (0.5, 5°)

(b) March-April with (λ, L) = (2, 1°)

(c) May-July with (λ, L) = (2, 1°)

(d) August-October with (λ, L) = (2, 1°)

Figure 18: Horizontal distribution of the depth of the DCM. (a) Background field obtained from a coarse analysis of the whole data set. The other figures are refined analyses for (b) March-April, (c) May-July and (d) August-October. White zones represent areas where the error field estimated by *DIVAnd* is above 50%. Vertical and horizontal colorbars (units: meters) represent, respectively, the values of the analyzed field obtained with *DIVAnd* and the observations, scattered on the map.

Figure 18 shows the distribution of the DCM with depth reconstructed with *DIVAnd* from March until October (*i.e.* where a DCM is present). Figure 18a shows the background field reconstructed (using all data points indifferently of seasons and years) from a global coarse analysis. The background highlights the presence of a longitudinal gradient of DCM depths with higher values from east to west except in the extreme west of the basin. Globally, the three periods are rather similar which would indicate the absence of seasonal variability at the depth scale. In March-April, maximum and minimum values are 52.5 m and 22.3 m for an average of 36.6 $\pm$ 7.4 m. The eastward longitudinal gradient starting at 28 m reaches its peak near 38 m before decreasing again to 34 m in the west. However, one has to keep in mind that reconstructed

values can be far from actual measured values due to the implementation of the variational analysis. The latter does not necessarily interpolate observations to take into account potential errors on data (*i.e* noise) and to deal with different observations at the same point as well as penalizes strong gradients (Troupin et al., 2013). Moreover, depth fields are highly influenced by the position of BGC floats. In this study, all data have been used indifferently of the years of collection. Hence, the spatial variability observed in Figure 18 can also be due to interannual variability. For instance, all floats were in the eastern basin in 2017 (Fig. 19) and it was the only year where this region was covered. Furthermore, some regions are not investigated by Argo floats such as the continental shelf in the northwestern part (too shallow, (Grayek et al., 2015)) or have not been explored yet (*e.g.* the extreme east of the basin). As a result, when doing pseudo-seasonal analyses, regions where the error field is greater than 50% were removed (white zones). In May-July, depths of DCM range between 15.6 and 50.8 m with a mean of 33.6 $\pm$ 8.0 m while in August-October, DCM range between 16.3 and 46.8 m for an average of 30.6 $\pm$ 5.6 m. As a whole, the mean depth of the DCM decreases from the beginning formation period (March) until the end (October). Although, pseudo-seasonal analyses are clearly influenced by the background and no specific structures arise from the distinct three periods including the center part where many data points are present between 2014 and 2016. This can supposedly be explained by several factors such as the high variability of DCM depths being constrained by *DIVAnd* analyses, the high variability in some regions (center of the basin for instance) over the years and the unequal yearly distribution of data points from floats (Fig. 19).

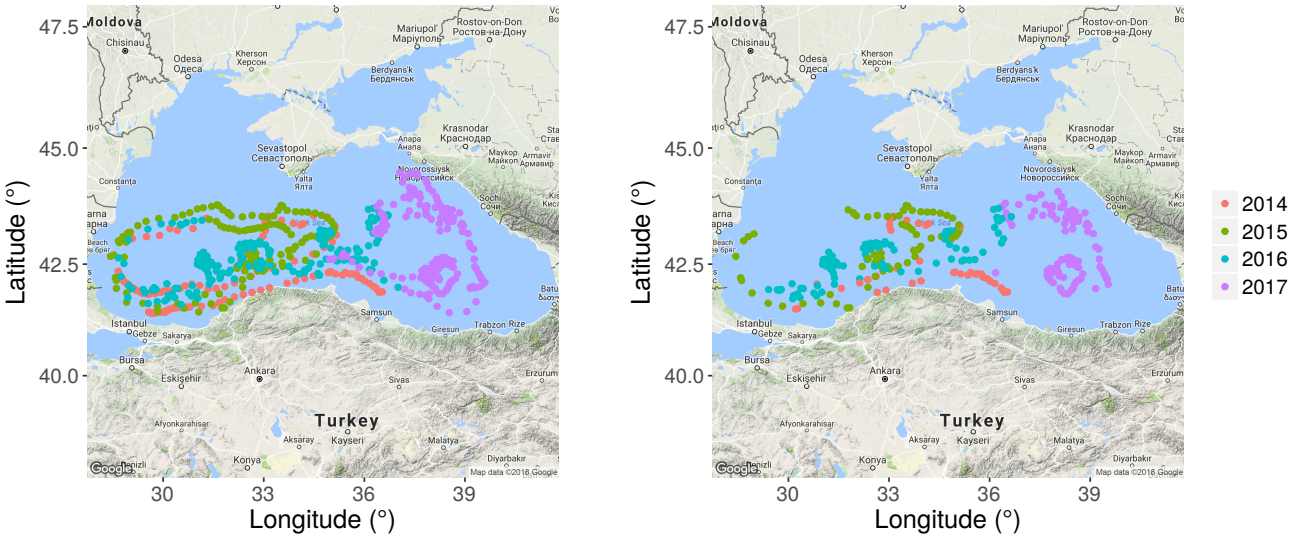

Figure 19: BGC-Argo floats trajectories in 2014-2017. Interannual positions of BGC-Argo floats (left) and interannual DCM and modified DCM distribution (right).

However, yearly DCM from April and May are always the deepest, generally $\approx$ 40 m (Fig. 20) independently of space. During this 4-year period, we notice that 2016, on average, had deeper DCM while we observed the contrary in 2017.

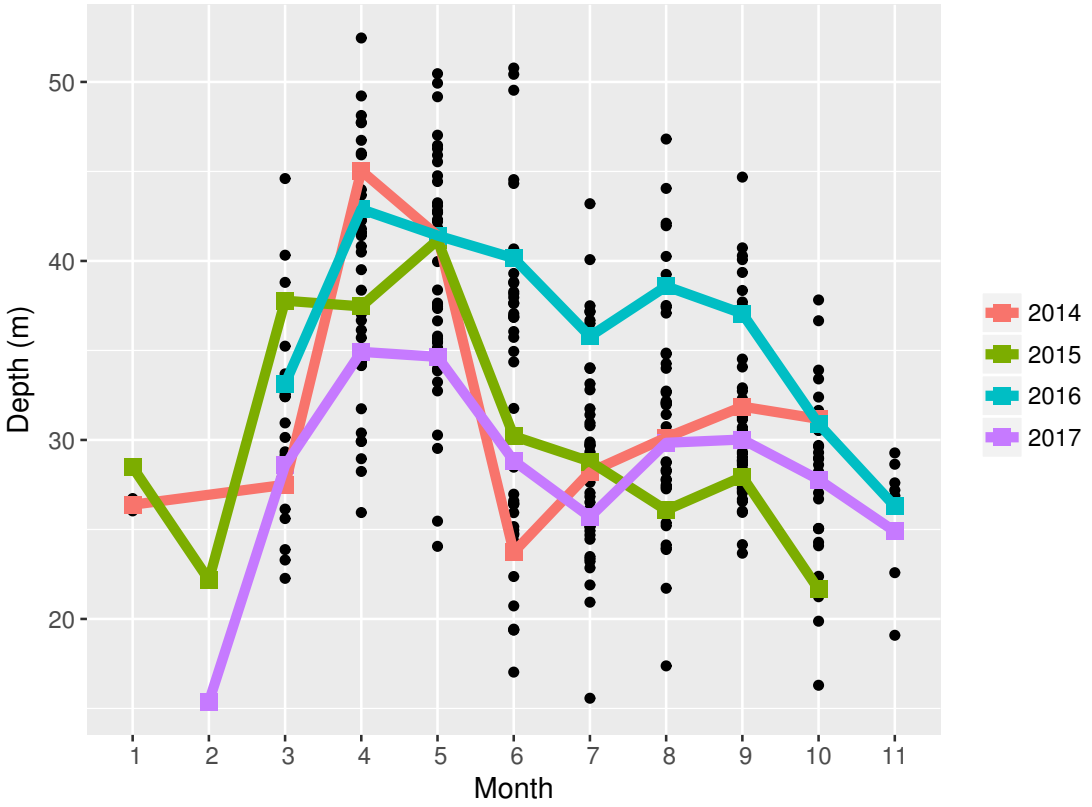

Figure 20: Monthly depths of DCM and modified DCM per year (black dots) with monthly averages per year.

4.3.2 Density analysis

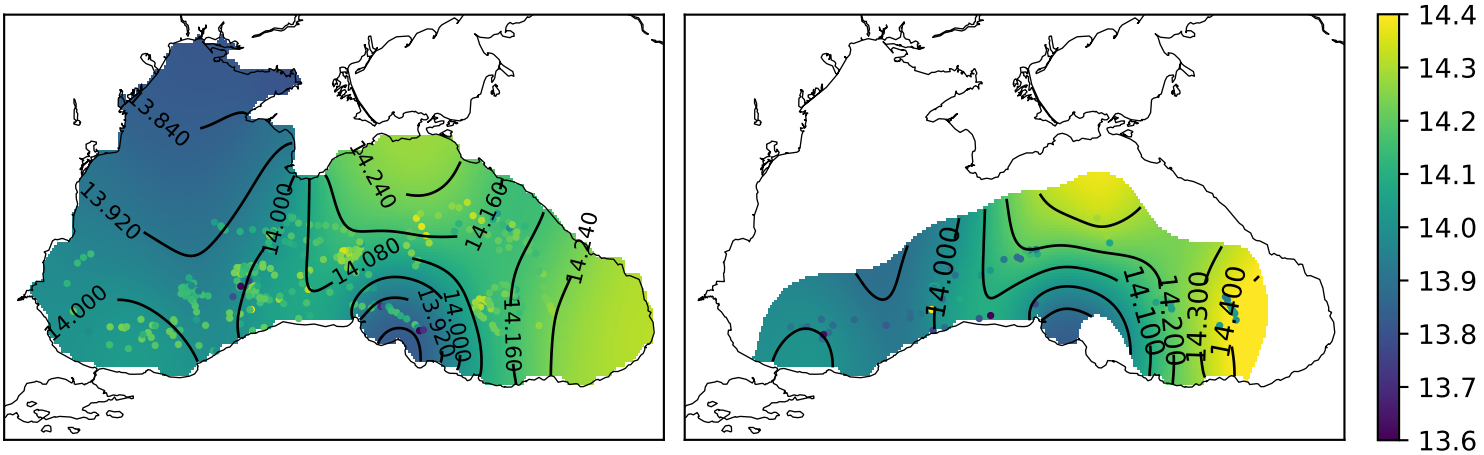

(a) Background with (λ, L) = (0.5, 5°)

(b) March-April with (λ, L) = (2, 1°)

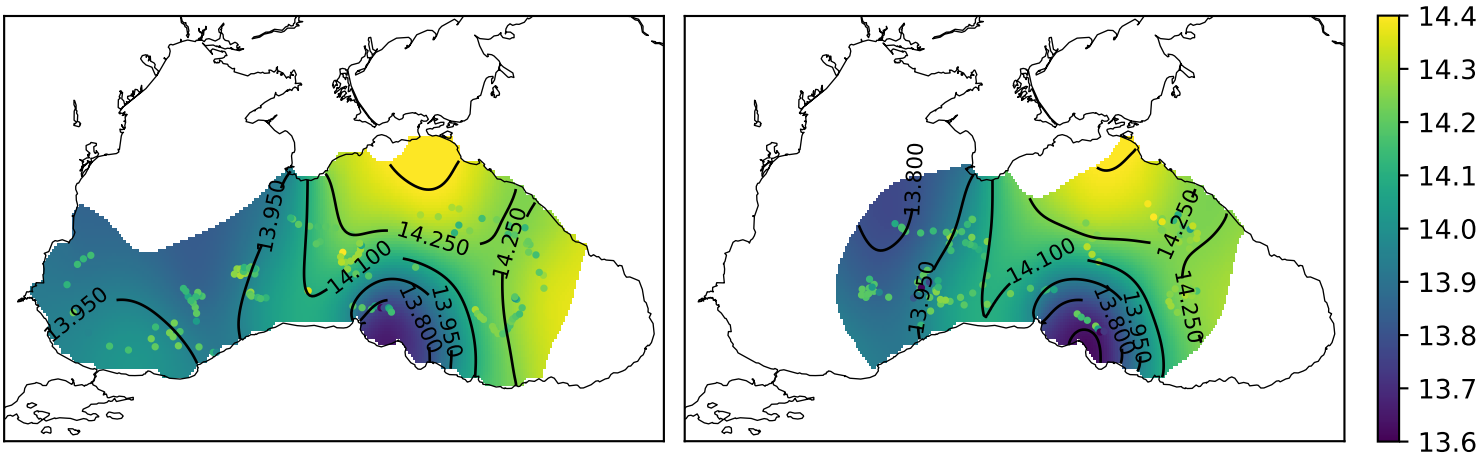

(c) May-July with (λ, L) = (2, 1°)

(d) August-October with (λ, L) = (2, 1°)

Figure 21: Horizontal distribution of the potential density anomaly of the DCM. (a) Background field obtained from a coarse analysis of the whole data set. The other figures are refined analyses for (b) March-April, (c) May-July and (d) August-October. White zones represent areas where the error field estimated by *DIVAnd* is above 50%. Observations are scattered on the map. The units of the colorbar are given in kg m^{-3}.

The background of the potential density anomaly positions of DCM is relatively smooth with a mean of 14.06 $\pm$ 0.37 kg m^{-3}. No major differences are observed for the three periods (as for the depth analysis). In March-April, a longitudinal gradient is observed with values decreasing westward from 14.4 to 14.0 kg m^{-3}. During this two-month period, σ_θ ranged between 13.82 and 14.93 kg m^{-3} with a mean of 14.35 $\pm$ 0.20 kg m^{-3}. In May-July, the decreasing westward gradient was still present (14.25 to 13.95 kg m^{-3}) except in a south-east central region (near the mouth of the Kizilmark river) where lower σ_θ were observed ($\approx$ 13.8 kg m^{-3}). Extreme range between 12.23 and 14.73 kg m^{-3} with an average of 14.06 $\pm$ 0.29 kg m^{-3}. In August-October, results were similar to the previous period with minimum and maximum values of, respectively, 11.90 and 14.65 kg m^{-3} with an average of 13.90 $\pm$ 0.43 kg m^{-3}. In a first approach, we can say that the general smoothness of the density field along with average values of $\approx$ 13.9 - 14.0 kg m^{-3} is coherent with what we have found about Navarro's hypothesis and the value of σ_θ of the winter mixed layer (where a bloom occurred). Surprisingly low values have been found in the May-July and August-October periods, nevertheless, average σ_θ and its standard deviation indicates that they are probably outliers or local

events. It would be interesting to see where those points are located and to analyze the shape of the DCM to see if this occurs only with a particular shape or not (modified DCM or DCM). Needless to say, we need a better spatio-temporal coverage to study the variability of the DCM at the interannual scale.

5 Discussion

5.1 VFDOM-based Chla profiles correction

In the Black Sea, CDOM appears to be responsible for the increase of Chla fluorescence with depth. It has already been shown that fluorescent DOM continuously increased with depth (*e.g.* Coble et al., 1991). Close to the surface, CDOM is degraded by sunlight (Kramer, 1979) and we have shown that the correction in the upper part of the water column is negligible compared to the deeper part (below the Chla minimum). In regards to the increase of CDOM with depth, data from BGC-Argo floats cannot discriminate its origin yet but the similarity of all CDOM profiles (shape and values) irrespective of time and space indicates that it could probably be from autochtonous origin (Zhang et al., 2009). The strong stratification of the Black Sea and the poor ventilation at depth (Bakan and Byükgüngör, 2000) also likely explain the uniformity of CDOM profiles at basin scale.

In order to try to quantify the quality of the correction brought by the virtual CDOM profile, a coarse sensitivity study was performed. For that purpose, three perturbation types were performed on the virtual CDOM profile: the first one consists in adding random noise to it, the second one addresses its shape with an increasing gradient with depth and the third one consists in implementing an arbitrary shape (hereafter referred to as twisted profile). This analysis shows that the FDOM-based algorithm is rather robust in the deeper part of the water column in the sense that no matter the perturbation of the virtual CDOM signal is, we obtain satisfactory results for Chla which approaches zero in the deep layer as expected (Fig. 23). In fact, this assessment can be explained by the algorithm of Xing et al. (2017) which makes the hypothesis that the relationship between Chla fluorescence and CDOM is linear and that it will always be possible, for realistic virtual profiles, to find a linear relationship between both variables in the depth calibration range, *i.e.* below the Chla minimum and the bottom (Fig. 22). Consequently, our hypothesis on the importance of the shape is not truly relevant, although it is better to keep a virtual profile similar to existing profiles to keep a satisfactory correction in the surface layer, otherwise the application of the VFDOM-method is irrelevant. Indeed, we show that virtual CDOM can be perturbed up to 30% without too much loss of precision in the surface layer (Table 5). It thus reinforces the robustness of the virtual profile taken by a simple averaging procedure. Furthermore, it can also be seen that by increasing the noise, slope_{FDOM} converges to 0, hence the recovery of the deep-offset method.

% noise	RMSE (mg m^{-3})	slope$_{FDOM}$ (mg m^{-3} ppb^{-1})	α (mg m^{-3})
0	0.010	0.019	0.002
5	0.010	0.019	0.002
10	0.010	0.019	0.004
25	0.010	0.017	0.014
30	0.011	0.017	0.013
35	0.012	0.016	0.022
40	0.014	0.016	0.026
50	0.017	0.015	0.034
75	0.028	0.011	0.057
100	0.036	0.009	0.074

Table 5: Perturbation of the virtual CDOM profile (% of random noise levels), linear regression coefficients (slope$_{FDOM}$, α) and RMSE for the surface layer in comparison to the correction with the real CDOM profile.

This linearity is verified in the Black Sea hence both regression coefficients are not so important for the deep water layer. On the other hand, it would be interesting to see if the hypothesis of linearity stands in other regions. Good study cases would be oxygen-limited regions with at least moderate levels of CDOM, for instance the Arabian Sea (Coble et al., 1998).

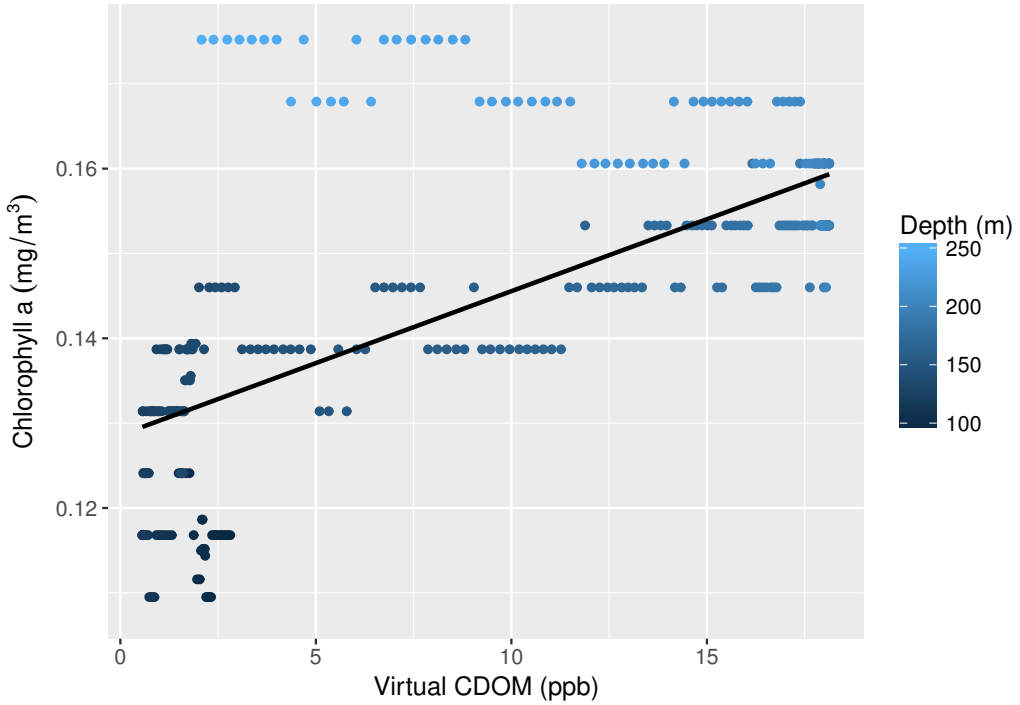

Figure 22: Scatterplot of CDOM versus Chla for the virtual twisted CDOM profile. In black, the linear regression line.

Consequently, we can establish three main results. Firstly, we have proved that the FDOM-based correction from Xing et al. (2017) works quite well in the Black Sea, especially in the deeper part of the water column when we compare with the HPLC profile taken at the deployment of the BGC-Argo float WMO 6903240. Secondly, the relative uniformity of CDOM profiles has allowed the construction of a representative - virtual - CDOM profile able to satisfactorily correct Chla profiles from every float in the Black Sea.

That being said, it would be interesting to search for CDOM profiles available in other areas to evaluate the linear relationship of CDOM and Chla because the main idea behind the algorithm relies on this supposition. Thirdly, the stagnancy of the open Black Sea likely insures the stability of CDOM at depth. In that perspective, it may be interesting to focus on other variables rather than CDOM for future floats, if it is now possible to correct Chla profiles without a CDOM fluorometer. Finally, this new method is highly experimental and has never been studied before, hence one should proceed with caution when implementing a virtual CDOM profile in regions different from the Black Sea.

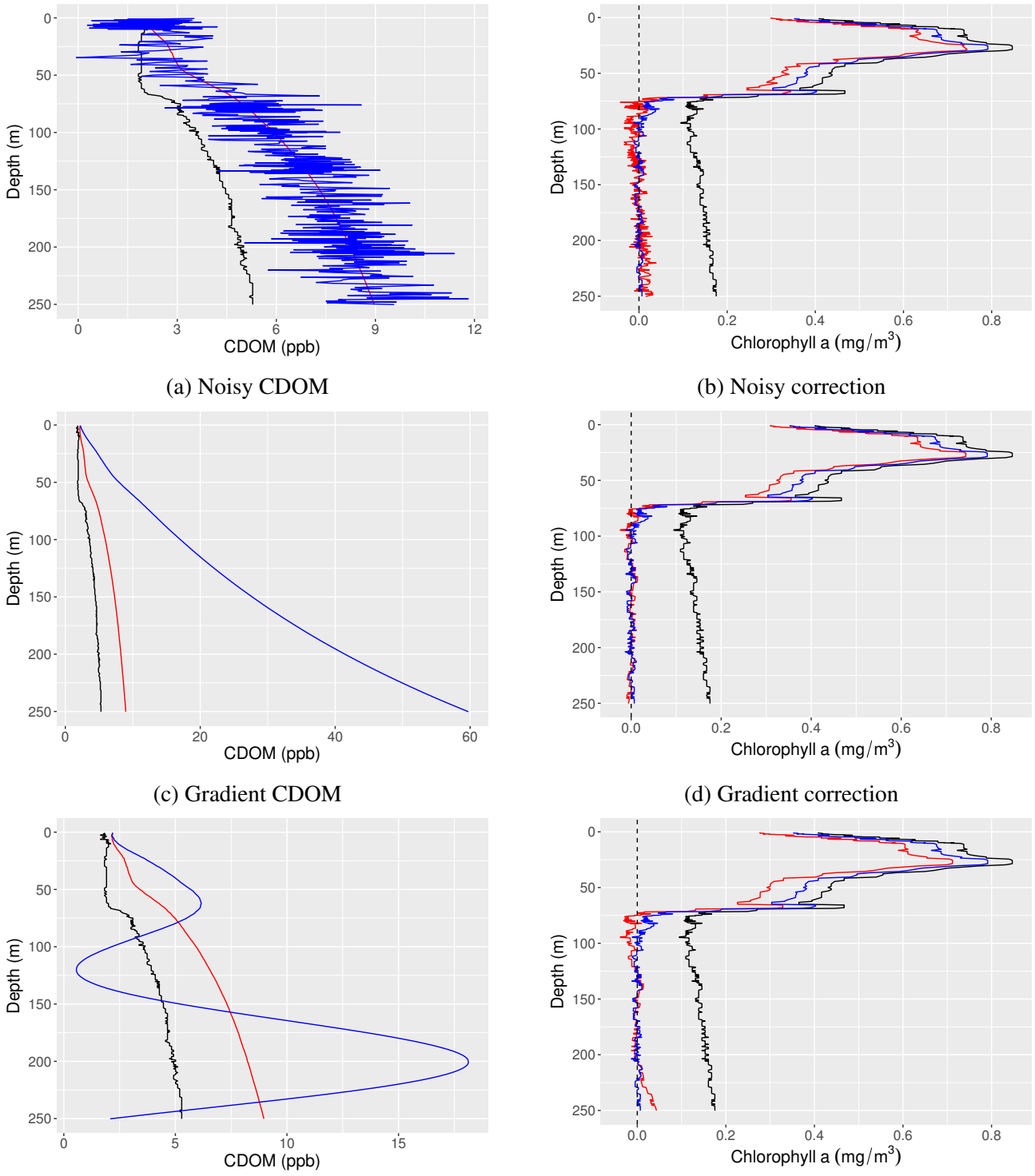

(a) Noisy CDOM

(b) Noisy correction

(c) Gradient CDOM

(d) Gradient correction

(e) Twisted CDOM

(f) Twisted correction

Figure 23: Different perturbation types (blue) of the virtual CDOM profile (red) compared to the real one (black).

5.2 DCM analyses

5.2.1 Depth analysis

The study of the three periods that we have defined using the histogram (Fig. 7b) agrees with the findings of Oguz et al. (1999). In other words, DCM seem to form after the winter/early spring bloom (below the

seasonal pycnocline), remain throughout summer and slowly deteriorate at the end of summer/early autumn (Vedernikov and Demidov, 1997; Oguz et al., 1999; Finenko et al., 2005; Yunev et al., 2005). The latter coincides with the deepening of the MLD and the weakening of the thermocline, allowing nutrient enriched waters from below to get to the surface (Oguz et al., 1996) but grazers could also be responsible for the DCM degradation (Mignot et al., 2014). The deepening of the MLD is likely involved in the degradation of well established DCM which are firstly hypothesized to be located at a depth where phytoplankton are not limited by nutrients from above and by light from below.

On the other hand, the high DCM variability with depth in the Black Sea, both spatially and temporally, has already been observed in previous studies (Finenko et al., 2005; Yunev et al., 2005; Oguz et al., 1999). In this study, highest average values were found in April-May ($\approx$ 40 m) similarly to Oguz et al. (1999) and Chu et al. (2005) while other months (from March to October, where DCM were observed, see Fig. 7b) generally presented DCM at depths between 30 and 40 m but sometimes up to 50 m as in Vedernikov and Demidov (1997) and Oguz et al. (1996, 1999). Such variability has also been observed in many other regions (Navarro and Ruiz, 2013; Green et al., 2014; Macías et al., 2014; Lavigne et al., 2015; Tripathy et al., 2015; Li and Hansell, 2017) and several explanations were proposed such as a light-driven DCM (Letelier et al., 2004), an isopycnal-driven DCM (Li and Hansell, 2017) sometimes associated to the pycnocline (Green et al., 2014; Lavigne et al., 2015) and more generally the nutrient-light intertwining conditions (Cullen, 2015).

Then, depth fields reconstructed after refined *DIVAnd* analyses did not show any seasonality. Only a deepening westward gradient was observed but its validity can be argued due to the data distribution (in space and time) as well as the quantity of data. Despite the fact that autonomous floats have a significant temporal sampling frequency and a high vertical resolution, contrarily to vessels measurements (Yunev et al., 2002), we have seen that the extension of the spatial coverage is also highly dependent on floats trajectories. Actually, an increasing eastward gradient has been observed in the Mediterranean Sea (Lavigne et al., 2015) but it seems that the longitudinal gradient obtained in our study has been highly influenced by the floats positions, especially in 2017 where observations show globally shallower DCM. In our opinion, the interpretation of the depth of DCM in the Black Sea using *DIVAnd* is made difficult by the lack of data, the high depth variability of DCM (Vedernikov and Demidov, 1997), in time and space, enhancing the spatial and temporal variability of the DCM. As a result, we have found a highly variable DCM without seasonality patterns or any structures governing it. In order to have more accurate results, more data are crucially needed and they must be ideally evenly distributed. Another possibility would be to use a detrending tool allowing to take into account the influence of spatial heterogeneity on the values obtained after *DIVAnd* analyses.

Regarding driving mechanisms of DCM, nitrate concentrations could not be used because they were too scarce to investigate a possible relationship between DCM and the nitracline (*e.g.* Letelier et al., 2004; Stanev et al., 2017). However, in the Black Sea, the nitrate maximum is on average located much deeper than the σ_θ of the DCM, at about 15.4 - 15.7 kg m^{-3} (Konovalov and Murray, 2001). Then, Vedernikov and Demidov (1997) found, in the open Black Sea, that the DCM was located near the 1% isolume and was observed deeper from spring to summer then ascended until the end of the year before disappearing.

Moreover, Yunev et al. (2005) also found a correlation between the Secchi depth (indicator of eutrophication) and the depth of the DCM. These observations would suggest a potential interaction with the light field. Likewise, Letelier et al. (2004) observed in the North Pacific Subtropical Gyre that DCM were closely associated to a PAR threshold of approximately 0.5 mol quanta m^{-2} d^{-1} all year long. Although their area of study does not concern temperate latitudes, it is compelling to search for potential similarities.

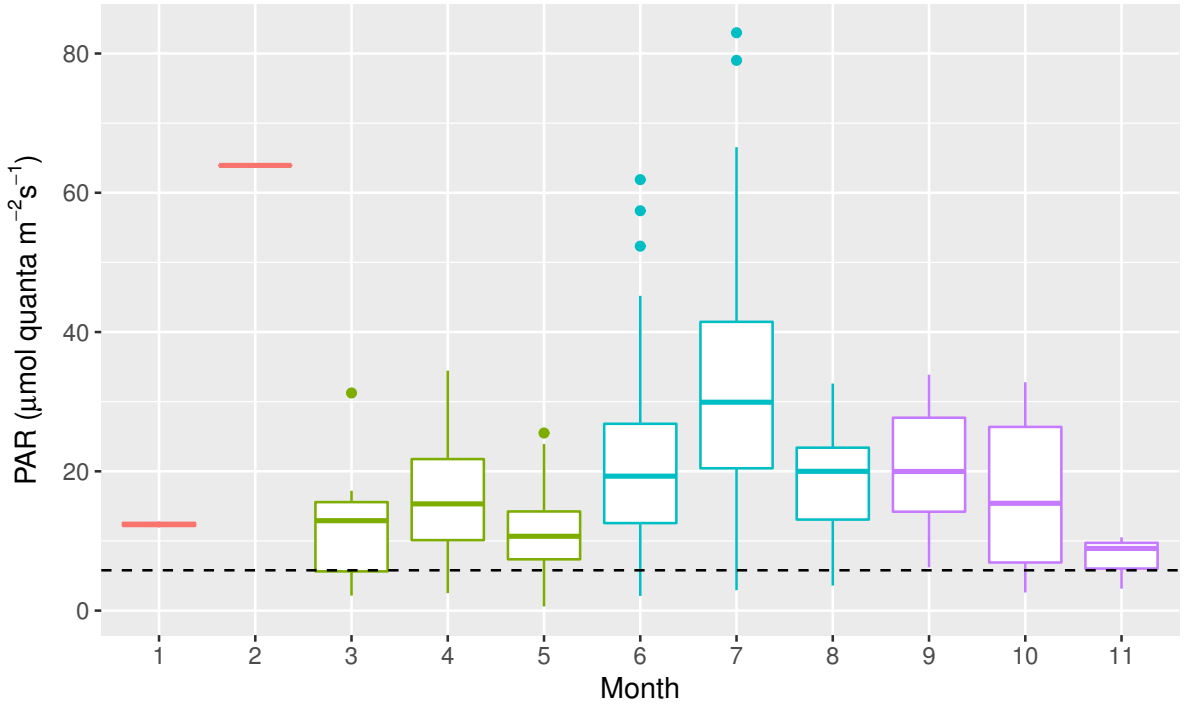

Figure 24: Distribution of the PAR value at the depth of the DCM (2014-2017 period). Colours depict seasons. The horizontal dashed bar represents the converted threeshold of 0.5 mol quanta m^{-2} d^{-1} in µmol quanta m^{-2} s^{-1}.

The instantaneous PAR is considered, in first approximation, as a reasonable indicator of the light field. It is quite clear from Figure 24 that DCM are not constrained by a specific PAR threshold. Mignot et al. (2014) already showed in the Mediterranean Sea that DCM followed a seasonal PAR threshold but it does not seem to occur in the Black Sea. The higher variability of temperate waters could be a reason explaining the fact that DCM are not constrained by a unique isolume threshold over the year due to less stable environmental conditions. Also, if DCM followed a particular isolume, we would expect a global deepening of DCM from spring till summer followed by a shallower DCM in autumn similarly to Vedernikov and Demidov (1997) and Mignot et al. (2014). It does not occur in our area of study (Fig. 24). Thus, the hypothesis of Letelier et al. (2004) stipulating that the DCM is light-driven at a specific threshold may not be adapted in all temperate regions and especially in the Black Sea which is a peculiar basin. Nevertheless, the fact that Vedernikov and Demidov (1997) found such a strong correlation between the 1% isolume, based on 15 years of collection (1978-1992), is surprising. Though their results are based on 140 stations, PAR data were measured with several sensors thus enhancing calibration discrepancies between them. Moreover, it was not always possible for them to compute directly the PAR hence empirical models were sometimes used, based on Secchi depth measurements.

5.2.2 Density analysis

The variability of DCM with σ_θ is much more constrained. This is not unexpected since the hysteresis hypothesis (Navarro and Ruiz, 2013) seems to be consistent with our observations (Fig. 16, 17 and 21). The deepest mixed layer is indeed found in January-February (Finenko et al., 2005). Additionally, Oguz et al. (1996) applied a model which again obtained deepest MLD in January-February when the winter convection is maximum with $\sigma_{\theta-surface}$ reaching 14.5 kg m^{-3} where observations at the time indicated 14.7 kg m^{-3}. Besides, Finenko et al. (2005) also observed that DCM occurred between densities of 11.8-14.2 kg m^{-3} (13.6 $\pm$ 0.53 kg m^{-3} in summer) which is coherent with our findings.

Consequently, our results show that the positions of DCM are generally close to the potential density anomaly of the (winter) maximum MLD. As a result, the settling of a DCM at such σ_θ could be due to a relic (final state) of the previous bloom (Stanev et al., 2017) occurring in winter/early spring (Yunev et al., 2002; Chu et al., 2005; Demidov, 2008; Finenko et al., 2014; Mikaelyan et al., 2017), that develops into a self-preserving structure (Beckmann and Hense, 2007), modifying its physico-chemical environment (Navarro and Ruiz, 2013), thus making its stay at such σ_θ feasible, before being degraded and gradually removed after October/November when turbulent events (deepening of the mixed layer, winter convection) arrive.

Other studies have also found a high correlation between DCM and a specific σ_θ (Green et al., 2014) with a great depth range thought to be related to oceanic mesoscale processes (Pasqueron De Fommervault et al., 2015), *e.g.* cyclonic structures which uplifts isopycnals. In order to see if the depth variability is indeed correlated to a strong isopycnal movement, we will focus on the data of the float WMO 6901866 for the year 2017 (Fig. 25).

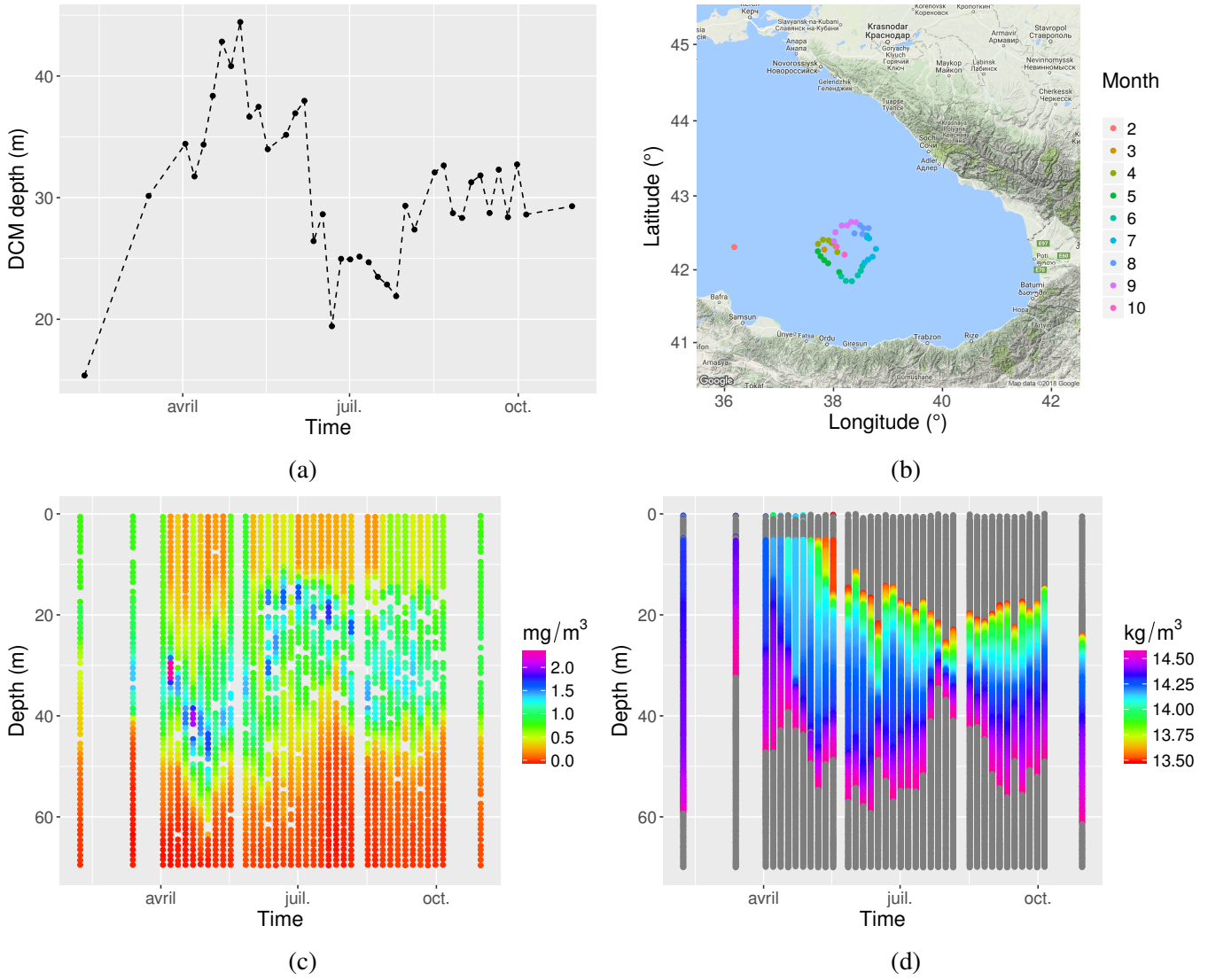

Figure 25: (a) Variability of the DCM with depth. (b) Float (WMO 6901866) trajectory in 2017. (c) Time series of Chla profiles. (d) Time series of potential density anomaly profiles. All data presented here coincide with the presence of a DCM or a modified DCM.

Between April and October, a DCM was present all the time (globally one profile every 5 days) at the location of the float which encompasses a relatively limited region. This case is interesting because for such a small region, the depth of the DCM rapidly changes over a short period of time, typically it goes up from approximately 40 m to 20 m in roughly 15 days (in June). Regarding data, a change of 20 meters is considered, in the Black Sea, as a significant change. However, this change does not seem to be related to a vertical movement of isopycnals. Furthermore, the DCM seems to follow an isopycne ($\approx$ 14.5 kg m^{-3}) consistent with the density of the winter mixed layer at first (until May) before rising up in the water column and leaving this layer. This change does not appear to be related, in first approximation, to light because we would expect a deepening of the DCM in the summer months.

Consequently, all those observations clearly show that DCM formation and maintenance is a dynamic and highly researched topic which has not delivered all its secrets yet. Though the hysteresis hypothesis suggested by Navarro and Ruiz (2013) needs more data, it still appears appealing, considering our results (see Fig. 16, 17 and 21) and because no obvious link with light has been highlighted either. Further studies

could focus on nitrate and PAR as well as quantitative aspects of Chla using BGC-Argo floats to improve our knowledge on the DCM in the Black Sea.

5.2.3 DCM shapes

Different DCM shapes have already been described (Uitz et al., 2006; Lavigne et al., 2015). In the Black Sea, Finenko et al. (2005) discussed four of them: homogeneous, unimodal (DCM), bimodal (double peak) and irregular profiles.

Homogeneous profiles (also referred as sigmoid profiles in this study) are dominant (Fig. 7a) during the cold period (December to March) due to important mixing convection (Finenko et al., 2005) while DCM dominate in the warmer period (May till October). April and November have been defined by Finenko et al. (2005) as transition zones between the two periods of colder and warmer temperatures in the upper water column. In our study, this transition seems to already take place in March where pseudo-Gaussian profiles exceed homogeneous profiles although DCM are way more established in April in terms of quantity. This is likely related to environmental conditions that may vary over the years (Kubryakov et al., 2016), especially the period of stabilization of the water column after the deep winter mixing. Throughout the summer, DCM clearly dominate the basin as in tropical and subtropical regions (Cullen, 1982). The degradation of unimodal profiles (DCM) seems to occur at the end of summer (September), however no sigmoid profiles were observed in August while Finenko et al. (2005) observed such profiles in all their stations at the same period. The deterioration continues in October until November where homogeneous profiles dominate again.

Lavigne et al. (2015) proposed that the modified DCM shape derived from the degradation of the DCM when deeper mixing occurs. However, we observed that the DCM in the Black Sea is non permanent and we propose that modified DCM encountered from January to March could come from the progressive establishment of the summer DCM instead. Furthermore, Lavigne et al. (2015) also stated that HSC profiles would coincide with bloom conditions in winter/early spring and autumn (Chu et al., 2005) but the highest frequency occurs in January whereas the first bloom of the year generally appears in late February/early March. A match-up with satellite data could be used to prove this assessment.

Seasonality studies on DCM are scarce (Mignot et al., 2014) and definitely more data are thus required to improve our understanding of phytoplankton dynamics.

6 Conclusion

Satellites cannot see below the optical depth but autonomous floats are able to study biogeochemical variables in the water column at a high vertical and temporal frequency thus accumulating an unprecedented amount of profiles for each period of the year, even in remote locations, highlighting unknown processes and confirming or disproving current theories in oceanography. In this study, we have shown that the FDOM-based method of Xing et al. (2017) to correct the monotonous increase of Chla with depth in the Black Sea is able to reconstruct the Chla profile in agreement with our HPLC data. On the other hand, for floats not endowed with a CDOM fluorometer, we have implemented a virtual CDOM profile, based

on the uniformity of existing CDOM profiles, able to correct their Chla profiles. This is made possible by the fact that the relationship between Chla and CDOM in the deep layer is indeed linear and because virtual CDOM can deviate from real CDOM by roughly 30% maximum in the surface layer to keep satisfactory results. In regards to our results, Chla profiles seem to be relatively homogeneous from November to February until the winter/early spring bloom occurs leading to the formation of modified DCM profiles. From April throughout summer, DCM are the dominant shape until early autumn where they are progressively degraded, increasing the number of modified DCM before disappearing in October when the mixing convection increases. In our study, the depth of the DCM showed significant variations but no seasonal variability was observed. Furthermore, DCM seem to be highly correlated to the density of the previous winter mixed layer, in all regions, hence the hysteresis hypothesis of Navarro and Ruiz (2013) seems to be consistent with our results. A limitation of our approach is that the density @max MLD, which corresponds to the density of the winter mixed layer, is estimated at the place and time of the DCM, although it should have been needed to consider the density @max MLD of the water mass where the winter bloom occurred. Moreover, no clear relationship between the depth of the DCM and PAR has been noticed contrarily to other studies in the Black Sea (Vedernikov and Demidov, 1997) and other temperate regions such as the Mediterranean Sea (Mignot et al., 2014; Lavigne et al., 2015).

Also, improvements of quality control procedures for CDOM and PAR are needed. In that perspective, it would be appreciated to have a database of high quality profiles (Organelli et al., 2017) updated on a daily basis for an easier use of BGC-Argo data and for an enhanced uniformity of profiles corrections among researchers. Again, it is clear that Chla measurements by fluorometry on autonomous platforms still remain a challenge. Several studies have already addressed some difficulties (IOCCG, 2011; Xing et al., 2012a; Roesler et al., 2017; Xing et al., 2017) but the high diversity of environments and phytoplankton species impedes fluorometers calibration.

In the future, it may be useful to equip more floats with sensors for highly variable parameters (e.g. Chla, PAR, nitrate). Indeed, we can reduce the amount of floats endowed with a CDOM fluorometer if the correction of Chla profiles with the virtual CDOM profile is judged to be satisfactory. Eventually, it would be interesting to increase the amount of BGC-floats in the Black Sea to further improve our knowledge on this particular basin.

Annexes

All scripts used for this study can be found on the Modelling for Aquatic Systems (MAST) repository on GitHub (https://github.com/MAST-ULiege/ArgoDiva) and can be quickly adapted to study other biogeochemical variables. A toolbox is currently under development to easily work with data from Argo floats (BGC and Core Argo). Its aim is threefold: designing a user-friendly script in order to be accessible to anyone working in natural sciences (especially oceanography), displaying several data visualization schemes and preparing input files for data interpretation with *DIVAnd*. Data analysis (see the material and method section) scripts are written in *R* while *DIVAnd* needs to be run on *Julia*. Scripts for data interpolation can then be run on *Jupyter Notebook*.

Acknowledgements

Argo data are collected and made freely available by the international Argo Program and by the national programs that contribute to it (http://www.argo.net).
All maps (except those created with *DIVAnd*) were created with the *ggmap* package (Kahle and Wickham, 2013).

References

G. Anderson. Subsurface chlorophyll maximum in the northeast Pacific Ocean. *Limnology and Oceanography*, 14(3):386–391, 1969.

M. Ardyna, M. Babin, M. Gosselin, E. Devred, S. Bélanger, A. Matsuoka, and J.-É. Tremblay. Parameterization of vertical chlorophyll a in the Arctic Ocean: impact of the subsurface chlorophyll maximum on regional, seasonal, and annual primary production estimates. *Biogeosciences*, 10(6):4383, 2013.

Argo Data Management Team. *Argo User's manual V3.2.*, 2017.

G. Bakan and H. Byükgüngör. The Black Sea. *Marine Pollution Bulletin*, 41(1-6):24–43, 2000.

A. Barth, C. Troupin, A. Alvera-Azcárate, L. Vandenbulcke, and J.-M. Beckers. Divand-1.0: N-dimensional variational data analysis for ocean observations. *Geoscientific Model Development*, 7(1):225–241, 2014.

A. Beckmann and I. Hense. Beneath the surface: Characteristics of oceanic ecosystems under weak mixing conditions–a theoretical investigation. *Progress in Oceanography*, 75(4):771–796, 2007.

Biogeochemical-Argo Planning Group. The scientific rationale, design and implementation plan for a Biochemical-Argo float array, 2016.

E. Böhm, F. Riminucci, G. Bortoluzzi, S. Colella, F. Acri, R. Santoleri, and M. Ravaioli. Operational use of continuous surface fluorescence measurements offshore Rimini to validate satellite-derived chlorophyll observations. *Journal of Operational Oceanography*, 9(sup1):s167–s175, 2016.

A. Capet, E. Stanev, J.-M. Beckers, J. Murray, and M. Grégoire. Decline of the Black Sea oxygen inventory. *Biogeosciences*, 13(4):1287–1297, 2016.

P. Chu, L. Ivanov, and T. Margolina. Seasonal variability of the Black Sea chlorophyll-a concentration. *Journal of Marine Systems*, 56(3-4):243–261, 2005.

H. Claustre, A. Sciandra, and D. Vaulot. Introduction to the special section bio-optical and biogeochemical conditions in the South East Pacific in late 2004: the BIOSOPE program. *Biogeosciences Discussions*, 5 (1):605–640, 2008.

H. Claustre, D. Antoine, L. Boehme, E. Boss, F. DOrtenzio, O. F. DAndon, C. Guinet, N. Gruber, N. O. Handegard, M. Hood, et al. Guidelines towards an integrated ocean observation system for ecosystems and biogeochemical cycles, 2009.

P. Coble, R. Gagosian, L. Codispoti, G. Friederich, and J. Christensen. Vertical distribution of dissolved and particulate fluorescence in the Black Sea. *Deep-Sea Research, Part A*, 38(Suppl. 2A):S985–S1001, 1991.

P. Coble, C. Del Castillo, and B. Avril. Distribution and optical properties of CDOM in the Arabian Sea during the 1995 Southwest Monsoon. *Deep Sea Research Part II: Topical Studies in Oceanography*, 45 (10-11):2195–2223, 1998.

J. Cullen. The deep chlorophyll maximum: comparing vertical profiles of chlorophyll a. *Canadian Journal of Fisheries and Aquatic Sciences*, 39(5):791–803, 1982.

J. Cullen. Subsurface chlorophyll maximum layers: Enduring enigma or mystery solved? *Annual Review of Marine Science*, 7:207–239, 2015.

J. J. Cullen. Diel vertical migration by dinoflagellates: roles of carbohydrate metabolism and behavioral flexibility. *Contrib Mar Sci*, 27(1):135–152, 1985.

C. de Boyer Montégut, G. Madec, A. Fischer, A. Lazar, and D. Iudicone. Mixed layer depth over the global ocean: An examination of profile data and a profile-based climatology. *Journal of Geophysical Research C: Oceans*, 109(12):1–20, 2004.

A. Demidov. Seasonal dynamics and estimation of the annual primary production of phytoplankton in the Black Sea. *Oceanology*, 48(5):664–678, 2008.

A. Dos Santos, M. d. C. Calijuri, E. Moraes, M. Adorno, P. Falco, D. Carvalho, G. Deberdt, and S. Benassi. Comparison of three methods for Chlorophyll determination: Spectrophotometry and Fluorimetry in samples containing pigment mixtures and spectrophotometry in samples with separate pigments through High Performance Liquid Chromatography. *Acta Limnol. Bras*, 15(3):7–18, 2003.

Z. Dubinsky and N. Stambler. Photoacclimation processes in phytoplankton: mechanisms, consequences, and applications. *Aquatic Microbial Ecology*, 56(2-3):163–176, 2009.

D. Ediger and A. Yilmaz. Characteristics of deep chlorophyll maximum in the Northeastern Mediterranean with respect to environmental conditions. *Journal of Marine Systems*, 9(3-4):291–303, 1996.

M. Estrada, C. Marrase, M. Latasa, E. Berdalet, M. Delgado, and T. Riera. Variability of deep chlorophyll maximum characteristics in the northwestern Mediterranean. *Marine Ecology Progress Series*, 92(3): 289–300, 1993.

K. Fennel and E. Boss. Subsurface maxima of phytoplankton and chlorophyll: Steady-state solutions from a simple model. *Limnology and Oceanography*, 48(4):1521–1534, 2003.

Z. Finenko, T. Churilova, and R. Lee. Dynamics of the vertical distributions of chlorophyll and phytoplankton biomass in the Black Sea. *Oceanology*, 45(SUPPL. 1):S112–S126, 2005.

Z. Finenko, V. Suslin, and I. Kovaleva. Seasonal and long-term dynamics of the chlorophyll concentration in the Black Sea according to satellite observations. *Oceanology*, 54(5):596–605, 2014.

K. Furuya. Subsurface chlorophyll maximum in the tropical and subtropical western Pacific Ocean: Vertical profiles of phytoplankton biomass and its relationship with chlorophylla and particulate organic carbon. *Marine Biology*, 107(3):529–539, 1990.

S. Grayek, E. Stanev, and J. Schulz-Stellenfleth. Assessment of the Black Sea observing system. A focus on 2005-2012 Argo campaigns. *Ocean Dynamics*, 65(12):1665–1684, 2015.

R. Green, A. Bower, and A. Lugo-Fernández. First autonomous bio-optical profiling float in the Gulf of Mexico reveals dynamic biogeochemistry in deep waters. *PLoS ONE*, 9(7), 2014.

Y. He, E. Stanev, E. Yakushev, and J. Staneva. Black Sea biogeochemistry: Response to decadal atmospheric variability during 1960-2000 inferred from numerical modeling. *Marine Environmental Research*, 77: 90–102, 2012.

J. Huisman, N. Pham Thi, D. Karl, and B. Sommeijer. Reduced mixing generates oscillations and chaos in the oceanic deep chlorophyll maximum. *Nature*, 439(7074):322–325, 2006.

IOC, SCOR and IAPSO. *The international thermodynamic equation of seawater - 2010 : Calculation and use of thermodynamic properties*. Intergovernmental Oceanographic Commission, Manuals and Guides No. 56, UNESCO (English), 196 pp., 2010.

IOCCG. *Bio-Optical Sensors on Argo Floats*. Claustre, H. (ed.), Reports of the International Ocean-Colour Coordinating Group, No. 11, IOCCG, Dartmouth, Canada., 2011.

K. Johnson, W. Berelson, E. Boss, Z. Chase, H. Claustre, S. Emerson, N. Gruber, A. Körtzinger, M. Perry, and S. Riser. Observing biogeochemical cycles at global scales with profiling floats and gliders: Prospects for a global array. *Oceanography*, 22(SPL.ISS. 3):216–225, 2009.

D. Kahle and H. Wickham. ggmap: Spatial Visualization with ggplot2. *The R Journal*, 5(1):144–161, 2013.

A. B. Kara, R. W. Helber, T. P. Boyer, and J. B. Elsner. Mixed layer depth in the Aegean, Marmara, Black and Azov Seas: Part I: general features. *Journal of Marine Systems*, 78:S169–S180, 2009.

S. Konovalov and J. Murray. Variations in the chemistry of the Black Sea on a time scale of decades (1960–1995). *Journal of Marine Systems*, 31(1-3):217–243, 2001.

C. Kramer. Degradation by sunlight of dissolved fluorescing substances in the upper layers of the eastern Atlantic Ocean. *Netherlands Journal of Sea Research*, 13(2):325–329, 1979.

A. Kubryakov, S. Stanichny, A. Zatsepin, and V. Kremenetskiy. Long-term variations of the Black Sea dynamics and their impact on the marine ecosystem. *Journal of Marine Systems*, 163:80–94, 2016.

H. Lavigne, F. D'Ortenzio, M. Ribera D'Alcalà, H. Claustre, R. Sauzède, and M. Gacic. On the vertical distribution of the chlorophyll a concentration in the Mediterranean Sea: A basin-scale and seasonal approach. *Biogeosciences*, 12(16):5021–5039, 2015.

R. M. Letelier, D. M. Karl, M. R. Abbott, and R. R. Bidigare. Light driven seasonal patterns of chlorophyll and nitrate in the lower euphotic zone of the North Pacific Subtropical Gyre. *Limnology and Oceanography*, 49(2):508–519, 2004.

Q. Li and D. Hansell. Mechanisms controlling vertical variability of subsurface chlorophyll maxima in a mode-water eddy. *Journal of Marine Research*, 74(3):175–199, 2017.

C. Lorenzen. A method for the continuous measurement of in vivo chlorophyll concentration. *Deep-Sea Research and Oceanographic Abstracts*, 13(2):223–227, 1966.

M. Macedo, P. Duarte, J. Ferreira, M. Alves, and V. Costa. Analysis of the deep chlorophyll maximum across the Azores Front. *Hydrobiologia*, 441:155–172, 2000.

D. Macías, A. Stips, and E. Garcia-Gorriz. The relevance of deep chlorophyll maximum in the open Mediterranean Sea evaluated through 3D hydrodynamic-biogeochemical coupled simulations. *Ecological Modelling*, 281:26–37, 2014.

J. Marra. Analysis of diel variability in chlorophyll fluorescence. *Journal of Marine Research*, 55(4): 767–784, 1997.

A. Mignot, H. Claustre, F. D'Ortenzio, X. Xing, A. Poteau, and J. Ras. From the shape of the vertical profile of in vivo fluorescence to Chlorophyll-a concentration. *Biogeosciences*, 8(8):2391–2406, 2011.

A. Mignot, H. Claustre, J. Uitz, A. Poteau, F. D'Ortenzio, and X. Xing. Understanding the seasonal dynamics of phytoplankton biomass and the deep chlorophyll maximum in oligotrophic environments: A Bio-Argo float investigation. *Global Biogeochemical Cycles*, 28(8):856–876, 2014.

A. Mikaelyan, V. Chasovnikov, A. Kubryakov, and S. Stanichny. Phenology and drivers of the winter–spring phytoplankton bloom in the open Black Sea: The application of Sverdrup's hypothesis and its refinements. *Progress in Oceanography*, 151:163–176, 2017.

J. J. Moré. The Levenberg-Marquardt algorithm: implementation and theory. In *Numerical analysis*, pages 105–116. Springer, 1978.

G. Navarro and J. Ruiz. Hysteresis conditions the vertical position of deep chlorophyll maximum in the temperate ocean. *Global Biogeochemical Cycles*, 27(4):1013–1022, 2013.

T. Oguz, H. Ducklow, P. Malanotte-Rizzoli, S. Tugrul, N. P. Nezlin, and U. Unluata. Simulation of annual plankton productivity cycle in the Black Sea by a one-dimensional physical-biological model. *Journal of Geophysical Research: Oceans*, 101(C7):16585–16599, 1996.

T. Oguz, H. W. Ducklow, P. Malanotte-Rizzoli, J. W. Murray, E. Shushkina, V. Vedernikov, and U. Unluata. A physical–biochemical model of plankton productivity and nitrogen cycling in the Black Sea. *Deep Sea Research Part I: Oceanographic Research Papers*, 46(4):597–636, 1999.

E. Organelli, M. Barbieux, H. Claustre, C. Schmechtig, A. Poteau, A. Bricaud, E. Boss, N. Briggs, G. Dall'Olmo, F. D'Ortenzio, E. Leymarie, A. Mangin, G. Obolensky, C. Penkerc'H, L. Prieur, C. Roesler, R. Serra, J. Uitz, and X. Xing. Two databases derived from BGC-Argo float measurements for marine biogeochemical and bio-optical applications. *Earth System Science Data*, 9(2):861–880, 2017.

A. Palazov, V. Slabakova, E. Peneva, and E. Stanev. Black Sea Argo: history, current status and prospect, 2014.

J. Para, P. G. Coble, B. Charrière, M. Tedetti, C. Fontana, and R. Sempéré. Fluorescence and absorption properties of chromophoric dissolved organic matter (CDOM) in coastal surface waters of the northwestern Mediterranean Sea, influence of the Rhône River. *Biogeosciences*, 7(12):4083–4103, 2010.

J. S. Parslow, P. W. Boyd, S. R. Rintoul, and F. B. Griffiths. A persistent subsurface chlorophyll maximum in the Interpolar Frontal Zone south of Australia: Seasonal progression and implications for phytoplankton-light-nutrient interactions. *Journal of Geophysical Research: Oceans*, 106(C12):31543–31557, 2001.

O. Pasqueron De Fommervault, F. D'Ortenzio, A. Mangin, R. Serra, C. Migon, H. Claustre, H. Lavigne, M. Ribera D'Alcalà, L. Prieur, V. Taillandier, C. Schmechtig, A. Poteau, E. Leymarie, A. Dufour, F. Besson, and G. Obolensky. Seasonal variability of nutrient concentrations in the Mediterranean Sea: Contribution of Bio-Argo floats. *Journal of Geophysical Research: Oceans*, 120(12):8528–8550, 2015.

T. Platt, S. Sathyendranath, C. M. Caverhill, and M. R. Lewis. Ocean primary production and available light: further algorithms for remote sensing. *Deep Sea Research Part A. Oceanographic Research Papers*, 35 (6):855–879, 1988.

C. Proctor and C. Roesler. New insights on obtaining phytoplankton concentration and composition from in situ multispectral Chlorophyll fluorescence. *Limnology and Oceanography: Methods*, 8(12):695–708, 2010.

J. Ras, H. Claustre, and J. Uitz. Spatial variability of phytoplankton pigment distributions in the Subtropical South Pacific Ocean: Comparison between in situ and predicted data. *Biogeosciences*, 5(2):353–369, 2008.

T. L. Richardson and J. J. Cullen. Changes in buoyancy and chemical composition during growth of a coastal marine diatom: ecological and biogeochemical consequences. *Marine Ecology Progress Series*, pages 77–90, 1995.

M. Rixen and J.-M. Beckers. A synopticity test of a sampling pattern in the Alboran Sea. *Journal of Marine Systems*, 35(1-2):111–130, 2002.

D. Roemmich, G. Johnson, S. Riser, R. Davis, J. Gilson, W. Owens, S. Garzoli, C. Schmid, and M. Ignaszewski. The Argo Program: Observing the global ocean with profiling floats. *Oceanography*, 22 (SPL.ISS. 2):34–43, 2009.

C. Roesler, J. Uitz, H. Claustre, E. Boss, X. Xing, E. Organelli, N. Briggs, A. Bricaud, C. Schmechtig, A. Poteau, F. D'Ortenzio, J. Ras, S. Drapeau, N. Haëntjens, and M. Barbieux. Recommendations for obtaining unbiased chlorophyll estimates from in situ chlorophyll fluorometers: A global analysis of WET Labs ECO sensors. *Limnology and Oceanography: Methods*, 15(6):572–585, 2017.

R. Röttgers and B. Koch. Spectroscopic detection of a ubiquitous dissolved pigment degradation product in subsurface waters of the global ocean. *Biogeosciences*, 9(7):2585–2596, 2012.

RStudio Team. *RStudio: Integrated Development Environment for R*. RStudio, Inc., Boston, MA, 2016.

C. Schmechtig, H. Claustre, A. Poteau, and F. D'Ortenzio. *Bio-Argo quality control manual for the Chlorophyll-A concentration*, 2014.

C. Schmechtig, A. Poteau, H. Claustre, F. d'Ortenzio, and E. Boss. Processing Bio-Argo chlorophyll-a concentration at the DAC level, 2016.

E. Stanev, Y. He, S. Grayek, and A. Boetius. Oxygen dynamics in the Black Sea as seen by Argo profiling floats. *Geophysical Research Letters*, 40(12):3085–3090, 2013.

E. Stanev, Y. He, J. Staneva, and E. Yakushev. Mixing in the black sea detected from the temporal and spatial variability of oxygen and sulfide – Argo float observations and numerical modelling. *Biogeosciences*, 11(20):5707–5732, 2014.

E. Stanev, S. Grayek, H. Claustre, C. Schmechtig, and A. Poteau. Water intrusions and particle signatures in the Black Sea: a Biogeochemical-Argo float investigation. *Ocean Dynamics*, 67(9):1119–1136, 2017.

E. Stanev, P.-M. Poulain, S. Grayek, K. Johnson, H. Claustre, and J. Murray. Understanding the Dynamics of the Oxic-Anoxic Interface in the Black Sea. *Geophysical Research Letters*, 2018.

E. V. Stanev. On the mechanisms of the Black Sea circulation. *Earth-Science Reviews*, 28(4):285–319, 1990.

D. K. Steinberg, N. B. Nelson, C. A. Carlson, and A. C. Prusak. Production of chromophoric dissolved organic matter (CDOM) in the open ocean by zooplankton and the colonial cyanobacterium Trichodesmium spp. *Marine Ecology Progress Series*, 267:45–56, 2004.

V. Taillandier, T. Wagener, F. D'Ortenzio, N. Mayot, H. Legoff, J. Ras, L. Coppola, O. P. de Fommervault, C. Schmechtig, E. Diamond, et al. Hydrography and biogeochemistry dedicated to the Mediterranean BGC-Argo network during a cruise with RV Tethys 2 in May 2015. *Earth System Science Data*, 10(1): 627, 2018.

S. Tripathy, S. Pavithran, P. Sabu, H. Pillai, D. Dessai, and N. Anilkumar. Deep chlorophyll maximum and primary productivity in Indian Ocean sector of the Southern Ocean: Case study in the Subtropical and Polar Front during austral summer 2011. *Deep-Sea Research Part II: Topical Studies in Oceanography*, 118:240–249, 2015.

C. Troupin, A. Barth, D. Sirjacobs, M. Ouberdous, J.-M. Brankart, P. Brasseur, M. Rixen, A. Alvera-Azcárate, M. Belounis, A. Capet, F. Lenartz, M.-E. Toussaint, and J.-M. Beckers. Generation of analysis and consistent error fields using the Data Interpolating Variational Analysis (DIVA). *Ocean Modelling*, 52-53:90–101, 2012.

C. Troupin, M. Ouberdous, D. Sirjacobs, A. Alvera-Azcárate, A. Barth, M.-E. Toussaint, S. Watelet, and J.-M. Beckers. *Diva User Guide*, 2013.

J. Uitz, H. Claustre, A. Morel, and S. Hooker. Vertical distribution of phytoplankton communities in open ocean: An assessment based on surface chlorophyll. *Journal of Geophysical Research: Oceans*, 111(8), 2006.

R. Varela, A. Cruzado, J. Tintore, and E. Garcia Ladona. Modelling the deep-chlorophyll maximum: a coupled physical- biological approach. *Journal of Marine Research*, 50(3):441–463, 1992.

V. Vedernikov and A. Demidov. Vertical distribution of primary production and chlorophyll during different seasons in deep regions of the Black Sea. *Oceanology*, 37(3):376–384, 1997.

A. Wong, R. Keeley, T. Carval, and the Bio Argo Team. *Argo Quality Control Manual for CTD and Trajectory Data*, 2018.

X. Xing, A. Morel, H. Claustre, D. Antoine, F. D'Ortenzio, A. Poteau, and A. Mignot. Combined processing and mutual interpretation of radiometry and fluorimetry from autonomous profiling Bio-Argo floats: Chlorophyll a retrieval. *Journal of Geophysical Research: Oceans*, 116(6), 2011.

X. Xing, H. Claustre, S. Blain, F. D'Ortenzio, D. Antoine, J. Ras, and C. Guinet. Quenching correction for in vivo chlorophyll fluorescence acquired by autonomous platforms: A case study with instrumented elephant seals in the Kerguelen region (Southern Ocean). *Limnology and Oceanography: Methods*, 10 (JULY):483–495, 2012a.

X. Xing, A. Morel, H. Claustre, F. D'Ortenzio, and A. Poteau. Combined processing and mutual interpretation of radiometry and fluorometry from autonomous profiling Bio-Argo floats: 2. Colored dissolved organic matter absorption retrieval. *Journal of Geophysical Research: Oceans*, 117(4), 2012b.

X. Xing, H. Claustre, E. Boss, C. Roesler, E. Organelli, A. Poteau, M. Barbieux, and F. D'Ortenzio. Correction of profiles of in-situ chlorophyll fluorometry for the contribution of fluorescence originating from non-algal matter. *Limnology and Oceanography: Methods*, 15(1):80–93, 2017.

E. Yakushev, V. Chasovnikov, J. Murray, S. Pakhomova, O. Podymov, and P. Stunzhas. Vertical hydrochemical structure of the Black Sea. *Handbook of Environmental Chemistry, Volume 5: Water Pollution*, 5 Q:277–307, 2008.

A. Yilmaz, D. Ediger, O. Basturk, and S. Tugrul. Phytoplankton fluorescence and deep chlorophyll maxima in the northeastern Mediterranean. *Oceanologica Acta*, 17(1):69–77, 1994.

O. Yunev, V. Vedernikov, O. Basturk, A. Yilmaz, A. Kideys, S. Moncheva, and S. Konovalov. Long-term variations of surface chlorophyll a and primary production in the open Black Sea. *Marine Ecology Progress Series*, 230:11–28, 2002.

O. A. Yunev, S. Moncheva, and J. Carstensen. Long-term variability of vertical chlorophyll a and nitrate profiles in the open Black Sea: eutrophication and climate change. *Marine Ecology Progress Series*, 294: 95–107, 2005.

Y. Zhang, M. A. van Dijk, M. Liu, G. Zhu, and B. Qin. The contribution of phytoplankton degradation to chromophoric dissolved organic matter (CDOM) in eutrophic shallow lakes: field and experimental evidence. *Water Research*, 43(18):4685–4697, 2009.

E. Özsoy and Ünlüata. Oceanography of the Black Sea: A review of some recent results. *Earth-Science Reviews*, 42(4):231–272, 1997.